Automated characterisation of Deep-sea imagery using Machine Learning: implications for future conservation and mineral extraction

Master Thesis in Earth Science

Marcos Tirado Barrio

Department of Earth Science

University of Bergen

June 2023

Abstract

This thesis aimed to develop a methodology using Machine Learning (ML) techniques for the interpretation of deep-sea resources. The deep-sea hosts diverse ecosystems and valuable resources, but potential environmental implications, particularly from mining activities, necessitate effective management strategies. Detailed maps of the sea floor are therefore a necessity, yet such maps have to date only been produced based on manual interpretation which is time consuming and subjective. The study focused on assessing the potential of ML methods to map deep-sea features based on photomosaic and bathymetry data in order to take the first steps in developing an automated, objective, and time-saving technique. This thesis's method accurately identified and classified features like chimneys at the hydrothermal vent fields, providing insights for resource interpretation and conservation.

Integrating ML methods into deep-sea resource management is crucial. The methodology enhances understanding of complex techniques, such as Convolutional Neural Networks (CNN) and Object-Based Image Analysis (OBIA) to overcome a seabed characterization. Simultaneously describing the parameters utilised to achieve a meaningful classification.

ML algorithms analyze large data volumes, extract patterns, and predict feature distributions, aiding targeted conservation measures and sustainable resource exploitation. The methodology successfully mapped hydrothermal chimneys in two study areas yet producer accuracies (0,7%) were higher than user accuracies (0,64%), indicating that there were other landforms that shared similar features.

The methodology also helps assess potential environmental implications of future mining, supporting informed decision-making and mitigation strategies. It serves also as a foundation for future research to aim at overcoming problems related to incomplete spatial coverage, attempt to better utilize shape and spatial parameters within the OBIA refinement, try to identify more background classes for excluding them from the model, etc.

Keywords: hydrothermal vent features, seabed exploration, object-based image analysis, seabed mining, environmental implications.

Master's Thesis in Earth Science, GEOV399, 60 credits
Supervisor: Benjamin Robson
Department of Earth Science (GEO), University of Bergen.

The whole document is available at https://bora.uib.no/bora-xmlui/

Acknowledgements

Special thanks to everyone who deserves it.

“But more wonderful than the lore of old men and the lore of books is the secret lore of ocean. Blue, green, grey, white, or black; smooth, ruffled, or mountainous; that ocean is not silent. All my days have I watched it and listened to it, and I know it well. At first it told to me only the plain little tales of calm beaches and near ports, but with the years it grew more friendly and spoke of other things, of things more strange and more distant in space and in time. Sometimes at twilight the grey vapours of the horizon have parted to grant me glimpses of the ways beyond; and sometimes at night the deep waters of the sea have grown clear and phosphorescent, to grant me glimpses of the ways beneath. And these glimpses have been as often of the ways that were and the ways that might be, as of the ways that are; for ocean is more ancient than the mountains and freighted with the memories and the dreams of Time.”

H.P. Lovecraft

Contents

Nomenclature

AI - Artificial Intelligence

AMOR - Arctic Mid-Ocean Ridge

AUVs - Autonomous Underwater Vehicles

CCZ - Clarion Clipperton Zone

CEDA - Central Dredging Association

CRS - coordinate reference system

CNNs - Convolutional Neural Networks

DSM - Deep Sea Mining

DOOS - Deep-Ocean Observing Strategy

EEZ - Exclusive Economic Zone

GEBCO - General Bathymetric Chart of the Oceans

GEOMAR - Helmholtz Centre for Ocean Research

GOOS - Global Ocean Observing System

ISA – International Seabed Authority

LSHVF – Lucky Strike Hydrothermal Vent Field

LCHVF – Loki's Castle Hydrothermal Vent Field

MAR - Mid-Atlantic Ridge

Ma - Million years ago

ML – Machine Learning

mbsl - metres below sea level

NOAA - National Oceanic and Atmospheric Administration

OBIA - Object-Based Image Analysis

PoW – plan of work

ROVs - Remotely Operated Vehicles

SDG - Sustainable Development Goals

Sonar - SOund NAvigation and Ranging

UN - United Nations

UTM - Universal Transverse Mercator

UNCLOS - United Nations Convention on the Law of the Sea

Thesis structure

Chapter 1: Introduction to the thesis topic, objectives, and research questions.

Chapter 2: General setting of the Mid-Atlantic Ridge and general background of the Hydrothermal Vent Fields.

Chapter 3: Theoretical background for image interpretation, deep learning, and eCognition software. Why this is a suitable method.

Chapter 4: Data Collection.

Chapter 5: Methodology used in this master thesis, the workflows followed to build the automated interpretation algorithm and the parameters utilised.

Chapter 6: Results obtained through the eCognition suite

Chapter 7: Discussion of results.

Chapter 8: Conclusion.

1. Introduction

1.1. History of deep-sea exploration

A relatively long tradition of the ocean exploration and monitoring results today in a worldwide integrated deep ocean observing system. It involves significant international cooperation, coordination, and agreements to create a bathymetric map of the entire ocean domain.

Ocean exploration companies and scientists use cutting-edge technology to collect bathymetry and photographic characterisation datasets to achieve this goal. This strategy uses strong data storage and transmission methods to ensure that the results are made publicly available quickly after data collection.

There are numerous examples of this kind of initiative: the Seabed 2030 project, on behalf of the General Bathymetric Chart of the Oceans (GEBCO), aggregates all available bathymetric data with the aim of producing the definite map of the global ocean floor by 2030. Or the Deep-Ocean Observing Strategy (DOOS), under the guidance of the Global Ocean Observing System (GOOS) (Levin et al., 2019), which seeks to bring together the global community of deep-ocean analysts in order to monitor and better understand the state of the deep ocean. These projects have benefited from the implementation of 21st-century autonomous technologies and are supported by numerous agencies and innovative enterprises.

There is a clear and growing interest in the deep sea, which can be explained by the following reasons. Firstly, this vast and unexplored frontier hosts a rich diversity of species and ecosystems. Many of these species are unique and have evolved to survive in extreme conditions, making them of great scientific interest. Secondly, the deep sea plays a crucial role in regulating the Earth's climate and supporting global ecosystems. Thus, it is of vital importance for understanding and mitigating the impacts of climate change. Finally, the deep sea is believed to be a potential source of valuable resources, including new minerals, oil, and gas exploitation opportunities (Cuyvers et al., 2018; Levin et al., 2019).

And yet, regardless of centuries of data collection and the development of new and better mapping technology in the past few decades, it is estimated that less than 18% of the global seafloor has been surveyed at a high resolution.

1.2. Natural diversity of the deep-sea

The deep ocean is defined as starting 200 metres below the sea level, known as The Twilight Zone, as very little light reaches this far below the sea. It is the largest environment on our planet in terms of volume and surface, yet also the least studied.

It is home to a unique marine diversity, as it is not found anywhere else with such specific conditions. The deep-sea hosts a type of biology and geology characterised by the influence of high pressures due to the depth, the absence of natural light and very low temperatures.

Figure 1. Interpretative collage of the deep-sea biodiversity. Pictures courtesy of NOAA, MBARI, and photographer Joshua Lambus.

Biologically, the seabed has a much higher biodiversity than previously thought. And even today, new species are still being discovered (Fig.1). This is indicative of the lack of knowledge that science has on this ecosystem and therefore how is directly affecting to its conservation. To work towards the objective of fulfilling SDG 14 - Life below water - of the Agenda 2030 for Sustainable Development, more precise seabed knowledge, particularly high-resolution bathymetric data, is necessary (Wölfl et al., 2019). Especially with regard to benthic species, bathymetry has proven to be one of the key driving tools for the study of species distribution. Aside from depth, derived variables including slope or roughness among others, they have been found to be important indicators in benthic species distribution models.

Similarly, reliable bathymetric models can have a significant impact on climate models' ability to replicate global events such as El Niño in the Pacific. Or the natural formation of tsunamis, closely linked to the morphology of the seafloor, such as the historic Storegga Slide on Norway's west coast (Kelley et al., 2015; Levin et al., 2019).

Geologically, and with special relevance for this thesis, the mining of three main minerals in the deep sea has been suggested for various types of habitats that can be found worldwide (Miller et al., 2018):

Manganese polymetallic nodules on the abyssal plains and Cobalt-rich crust at seamounts have their most significant deposits in the Pacific Ocean, with a notable concentration along the Clarion-Clipperton Zone (CCZ). Polymetallic sulphides are found at hydrothermal vents, including those along the Mid-Atlantic Ridge (Fig 2).

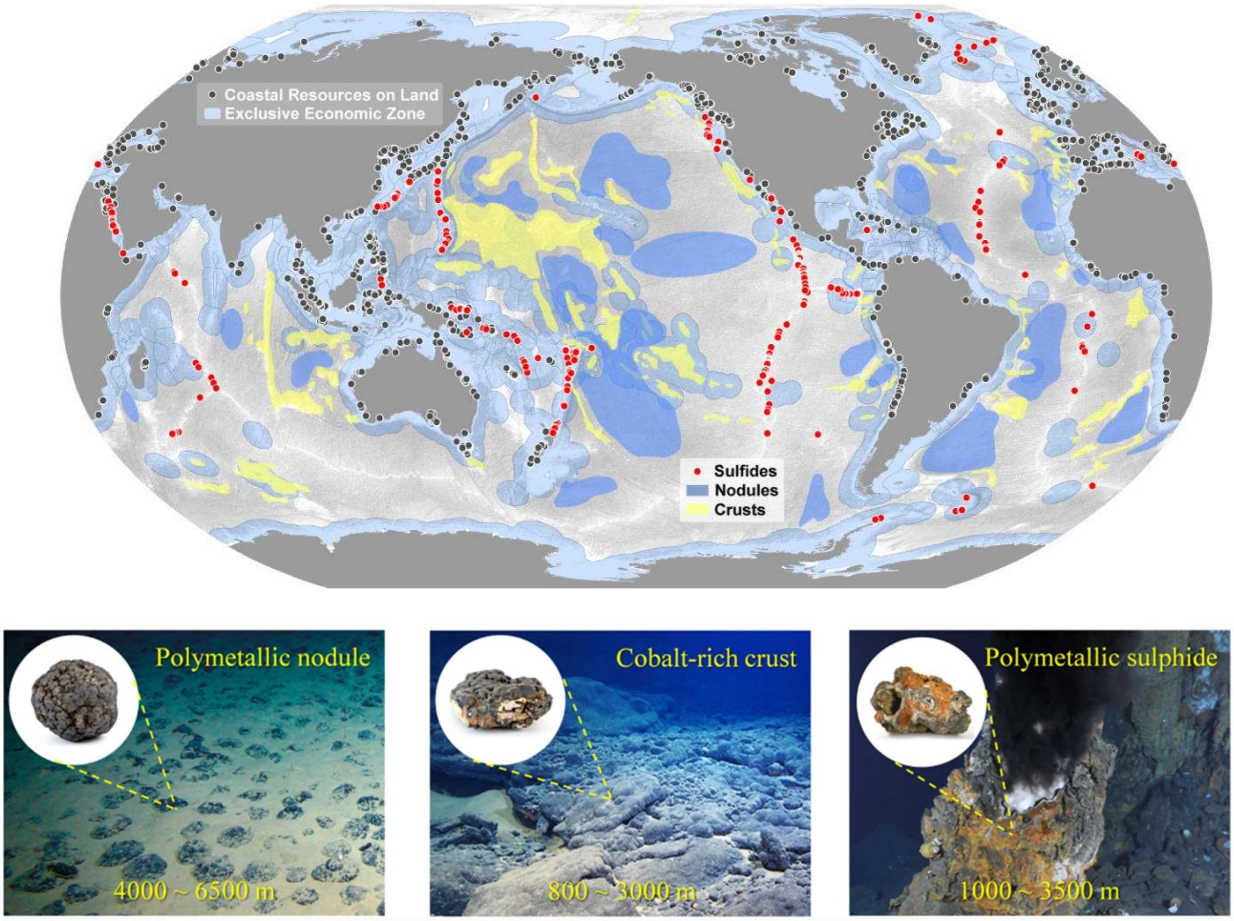

Figure 2. Mineral resources distribution, and representative images of three major deep seabed mineral resources. Pictures courtesy of GEOMAR and (Guo et al., 2023)

- Manganese polymetallic nodules on the abyssal plains: Structures compound primarily of manganese and iron together with traces of other commercially relevant metals such as nickel, copper, and rare earth metals among others. The nodules present a potato-like shape in which minerals are deposited around a solid nucleus. It takes millions of years for these nodules to grow up to 4 to 10 centimeters in diameter.

- Cobalt-rich crust on the slopes and top of seamounts (underwater mountains): Also known as ferromanganese crust, they are formed through the precipitation of minerals dissolved in seawater onto sediment-free substrates and are composed by a variety of trace metals such as manganese, iron, cobalt, nickel, and platinum. Due to its numerous applications in superalloys, and battery technology, cobalt is a subject of significant commercial interest.

- Polymetallic sulphides on the hydrothermal vents: Formations containing a high sulphide concentration but are also abundant in copper, zinc, gold, lead, barium, and silver. They are connected to either ongoing or extinct hydrothermal activity along the oceanic ridges. According to the findings of the exploration and resource evaluation, it has been estimated that approximately 10 potential deposits out of over 200 mineralized sites may possess enough grade to be considered suitable for commercial mining.

The discussion will provide a more detailed description of how these features interact within their respective habitats.

1.3.Impact of human activity on deep-sea ecosystems

Mapping the seafloor has the potential to meet the increasing global demand for more minerals and metals. The depletion of the resources located on land, has led to a renewed search for new metal supply chains, i.e., deep-sea mining. Despite not having started the extraction as such yet, exploration licenses for these resources have already been given to private investors and research institutions of multiple nationalities (Miller et al., 2018).

At this early stage of the process, new data collection techniques are essential for assessing the feasibility of mining initiatives. Furthermore, the accuracy of this data is important in order to obtain a complete grasp of what is lying at such depths, where technological disadvantages like the absence of light and the challenging accessibility, or even the lack of regulations makes it harder to govern these potential activities.

Regarding conservation efforts, new maps can be used to identify important habitats and to design marine protected areas. Accurate maps of the seafloor are important for understanding the geology and ecology of the deep sea, as well as for predicting the impacts of climate change and other environmental factors.

Thus, there is a growing need to address the knowledge gap that now exists around the potential environmental impacts of possible industrial activity in the deep-sea. In this paper, support vessel operations, shipping risks and accidents are not addressed. For the moment, no metalliferous resource has been fully mined, hence not all mining consequences are based on scientific findings. Small-scale perturbations or shallow water processes can suggest some impacts, but others are hypothetical (Christiansen et al., 2020; Miller et al., 2018):

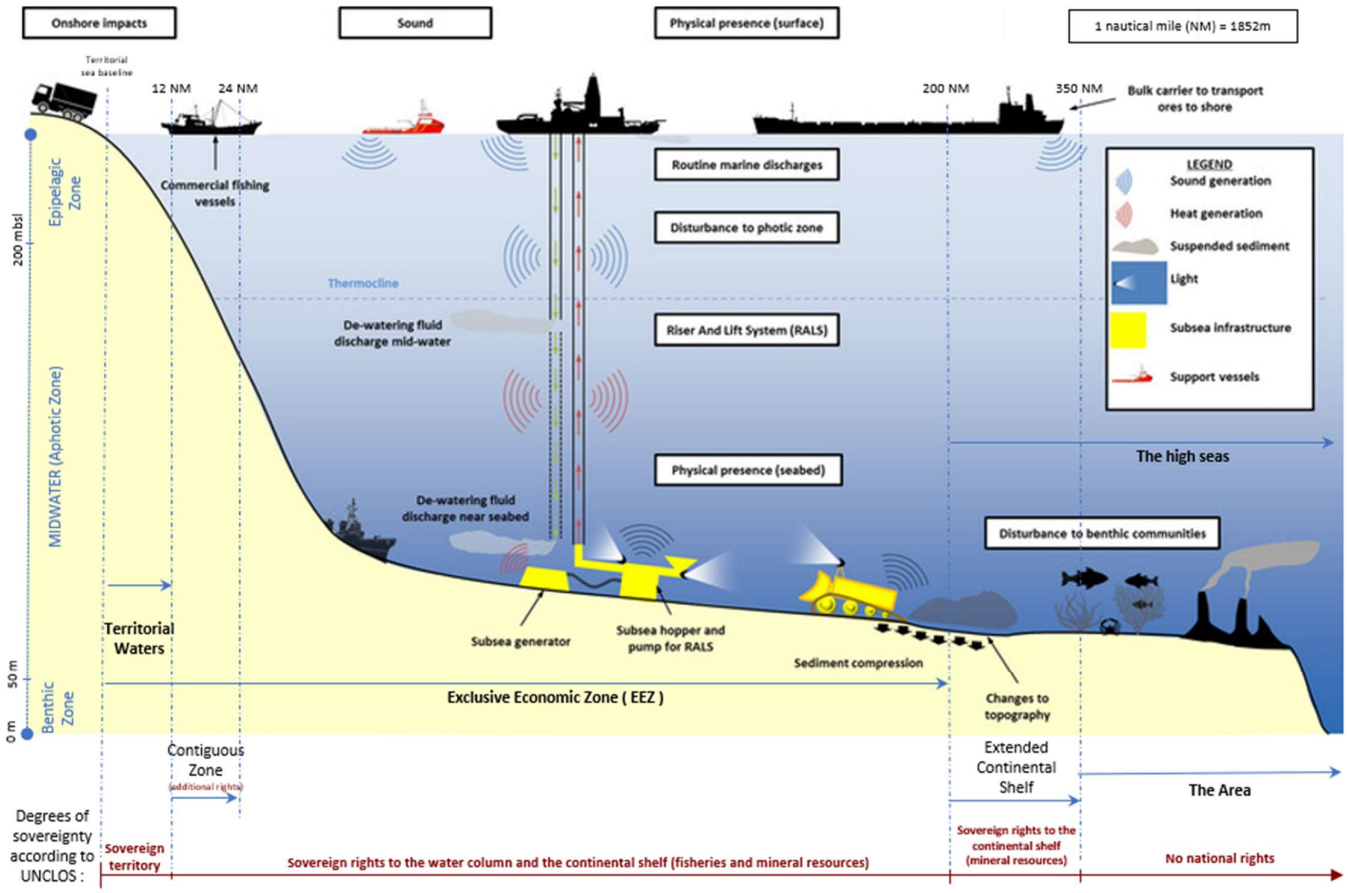

Figure 3. Classification of diverse depths, distinct maritime zones along with their corresponding national sovereignty rights, and different maritime resources. Modified from CEDA deep sea mining information portal. (Koschinsky et al., 2018; Miller et al., 2018)

A removal of substrate, caused by cutting, scraping, and dragging of ore deposits and sediments, could affect broad sections of the seafloor, depending on which resources are being

extracted. Following that, the majority of potential mining scenarios these days include a closed riser mechanism that requires substantial volumes of ambient water to dilute the soil and the crushed ore and transport the resulting slurry to the surface. Similarly, significant amounts of surface water will be transferred to benthic regions. Meaning that both habitats will be altered, potentially leading to the infiltration of non-native organisms or harmful substances that may, in particular cases, be able to survive the abrupt change in scenarios.

This part of the procedure results in the creation of two distinct categories of sediment plumes. The operational aspect is attributed to the utilisation of mining equipment and the motion of collectors positioned on the ocean floor. The second factor, which has a further significant influence, involves the creation of sediment plumes upon discharge. Such plumes will reach unpredictable heights or lengths, and are dependent on many variables, including the dimensions of the particles in suspension, the prevailing oceanic currents, and the topography of the ocean floor. The altered sediment deposition rate will have an impact on all deep-sea fauna that lacks the ability to feed under these new conditions.

Furthermore, the process of extracting ore from rock involves the leaching of heavy metals, which could be performed on the mining vessel during a primary stage. However, if these heavy metals are subsequently dumped back into the ocean, they may release significant amounts of toxic substances into the sediment plumes. The potential side effects of acidification and oxygen depletion resulting from industrial activity have received limited research attention, as no such activity has yet started.

Collectors for manganese nodules, cobalt crust and massive sulphides will likely have powerful lights to illuminate the seafloor along the mining path for camera control. Survey, inspection, and maintenance ROVs will also emit more light. However, many fishes and invertebrates with fully developed eyes are likely sensitive to bioluminescence's low light levels (Fig 1). Bioluminescence is the only natural light source in the deep water and found in all seas. Bacteria and fish produce it, and certain species of fish are drawn towards light, while others exhibit negative response to light stimuli. The tendency to be drawn towards light could potentially amplify the risk of entrainment, among other hazards. Bright illumination can locally cover up the ecological function of bioluminescence.

The exact role of sound within deep-sea ecosystems remains largely unknown. The propagation of noise generated during ore extraction can have a significant impact on vast regions due to the omnidirectional nature of underwater sound dispersion, particularly at low frequencies, potentially spanning hundreds of kilometres.

With the above, the precise mapping of the seabed holds great significance and a crucial responsibility in the initial stages of determining the possible viability of a mining project, given the number of potential impacts involved. One of the mapping responsibilities refers to the modelling of plume behaviour, which is heavily influenced by the topography of the seafloor. Alternatively, it also involves gathering the most effective paths for the collectors. The process requires the determination of optimal routes for collectors, which takes into account the location of high populated areas or submerged landforms that may serve as obstacles, thereby reducing the potential adverse effects on the ocean floor.

1.4. Goals, objectives, and research questions.

This thesis aims to broaden the perception of the deep marine environments by testing CNNs and OBIA specifically for deep-sea imagery and to determine if artificial intelligence can more efficiently characterise the ocean floor, which can be useful in assisting researchers in better understanding how human activities, such as pollution and climate change, affect the oceans. To accomplish this goal, the next steps were followed:

1. To determine what level of pre-processing is needed in order to robustly and consistently apply machine learning algorithms on deep sea imagery.
2. To assess what model structure is most suitable for interpreting deep sea imagery, as well as what geological forms meet the conditions to be the most appropriate to be recognised by the model.
3. To expand on whether it is possible to scale up this methodology over larger extends with the existing resources.
4. To consider the bigger picture of what automated analysis of deep-sea imagery could mean, and how such techniques can help contribute to more effective habitat management and monitoring.

2. Geological Setting

2.1. Mid Ocean Ridges formation

The scientific concept of plate tectonics illustrates the dynamic motion of the Earth's crustal plates and the resulting geological structures that arise from their interactions. The Mid-Ocean Ridges, a lengthy range of mountains spanning the Earth's oceanic basins, is regarded as a highly characteristic attribute of this particular theory. These locations are crucial for comprehending the tectonic mechanisms, as they represent the sites where new oceanic crust is generated. (Alt, 1995; Dyment et al., 2007).

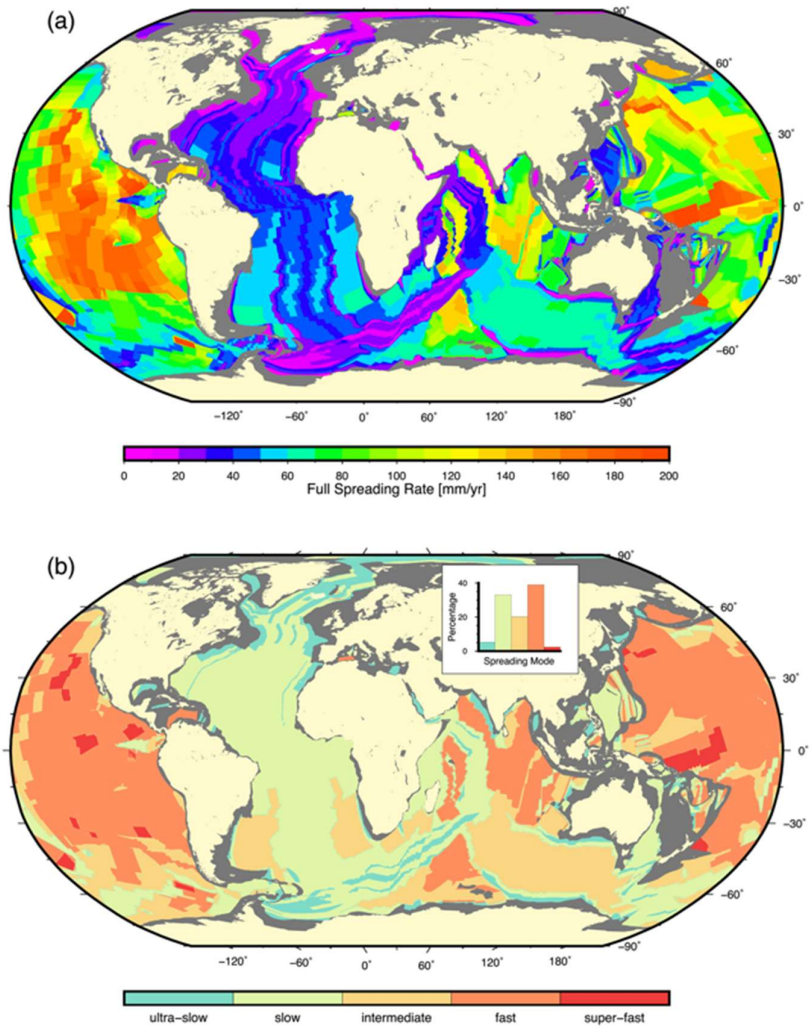

Figure 4. (a) The current seafloor spreading rate grid. (b) The current spreading mode grid. Ultraslow (<20 mm/yr), slow (20–55 mm/yr), intermediate (55–75 mm/yr), fast (75–180 mm/yr), and super-fast (>180 mm/yr). Histogram insert shows the percentage of each spreading mode. (Seton et al., 2020)

The emergence of the Mid-Ocean Ridges is an indication of continental drift, specifically when divergent plate boundaries are spreading apart. When two tectonic plates diverge, magma ascends from the Earth's mantle to occupy the space between them. As the molten rock known as magma experiences cooling and solidification, it results in the formation of fresh oceanic crust that subsequently builds up to the edges of the tectonic plates (Tivey, 2007). Over a period of time, this phenomenon leads to the development of the extended and uninterrupted series of submerged mountains that traverse the oceanic basin.

Several research methodologies have been employed to improve the understanding of the relationship between plate tectonics and the formation of the Mid-Ocean Ridge. The techniques included in this set of methods consist of seafloor cartography, seismic profiling, and borehole drilling. (Seton et al., 2020). Studies have provided important insights regarding the configuration and constitution of the Earth's crustal plates, along with the geological mechanisms that facilitated the genesis and also predict the evolution of the Mid-Ocean Ridges.

Volcanic activity is occurring frequently, particularly in close proximity to the spreading centres where tectonic plates are diverging. This process creates seamounts, volcanic islands, and other topographical characteristics that are discernible on the ocean floor, such as the hydrothermal vent fields.

2.1.1. Mid-Atlantic Ridge

The Mid-Atlantic Ridge (MAR) is an extensive underwater mountain range that extends across the Atlantic Ocean from 87° N to 54° S. This entity is an outcome of tectonic activity and is distinguished by its division into multiple ridge segments that show a right-stepping pattern. These segments vary in length, spanning from ten to hundreds kilometres. (Bramley et al., 2019). The MAR defines the boundary separating the North American Plate and the Eurasian Plate, experiencing an average spreading rate of approximately 22 mm/year (Eason et al., 2016) making it one of the most active volcanic and hydrothermal systems on the planet.

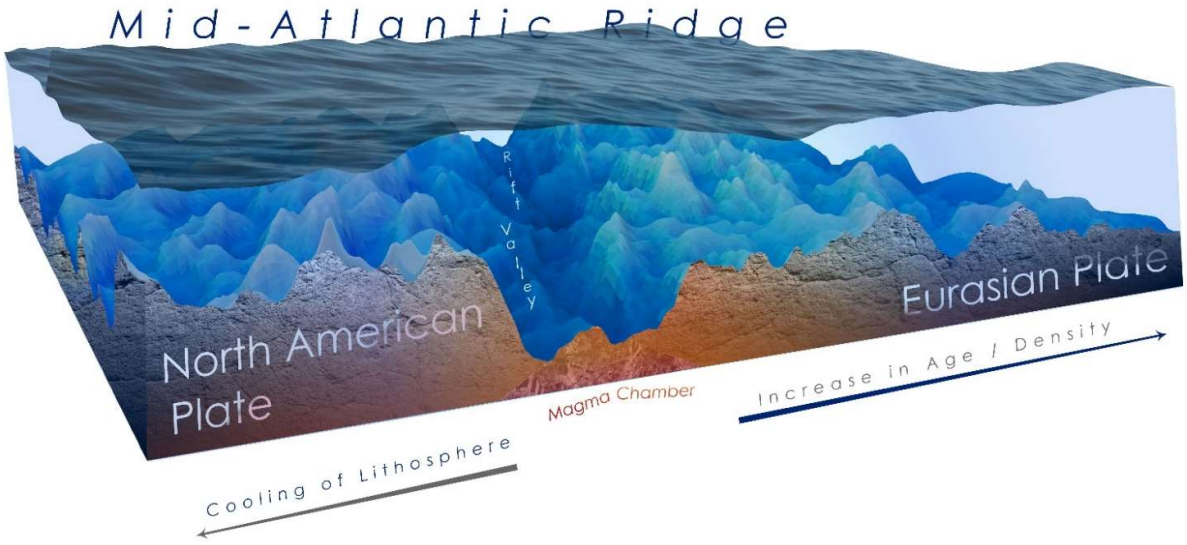

Figure 5. MAR setting interpretation

The genesis of this geological formation is explained by its positioning on a magmatic bulge that spans the Atlantic Ocean, upon which the mid-oceanic ridge is situated. The emergence of this protuberance was triggered by a surge of convective forces coming from the asthenosphere, which allowed the production of newly formed lithosphere and oceanic crust. The geological incident actually happened in the Triassic period (201 Ma-252 Ma), in which a sequence of three-armed grabens converged on the supercontinent Pangaea. It is expected for a divergent plate boundary to form in only two segments of a three-armed graben. The geological term for the "failing arms" is aulacogens. The aulacogens of the MAR have contributed to the formation of the river valleys present today across the continents of Africa

and the Americas. Examples of such river valleys include the Mississippi, Amazon, and Niger rivers (Burke, 1976; Burke & Wilson, 1976; Humphris et al., 2002).

The MAR presents a diverse range of lithologies that hold significant implications for the understanding of plate tectonics and the formation of the oceanic crust. Basalts, serpentines, gabbros, and dolerites show unique chemical compositions and physical characteristics (Fig 6), which offer valuable insights into the sub-surface processes of the ocean. (Dick et al., 2003). Understanding these lithologies is essential for improving the comprehension of the Earth's crust and the mechanisms that facilitate the formation of hydrothermal vents (Emery & Uchupi, 2012; Fox et al., 1973; Nicholls et al., 1964):

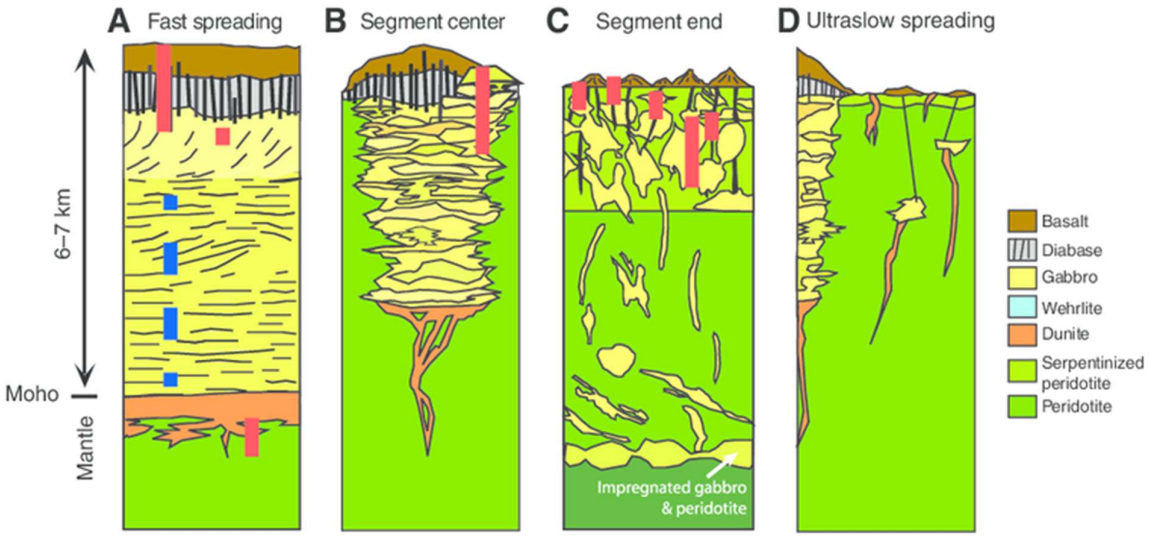

Figure 6. Ocean ridge crustal accretion models. A - Classic interpretation of the Penrose Model for a fast-spreading ridge; B - Penrose model modified for slow-spreading ridges based on the abundance of peridotite and frequent absence of gabbro at transforms following focused melt-ow models; C - Model of the anomalous 14-16°N area of the Mid-Atlantic Ridge; D - Model of the magmatic and amagmatic accretionary segments at ultraslow-spreading ridges Red and blue bars are drilling sites and targets respectively (Dick et al., 2003).

-Basalts represent a prevalent lithological type that is frequently found in the MAR, constituting an important portion of the oceanic crust. These rocks are characterised by their dark colour and fine-grained texture and are the result of the solidification of lava that has been extruded onto the oceanic crust. Basaltic rocks are primarily composed by minerals such as plagioclase feldspar, pyroxene, and olivine, and possess a relatively low silica content. Basaltic rocks exhibit a relatively homogeneous aspect, characterised by diminutive mineral grains that are difficult to discern with the naked eye.

- Serpentines represent a distinct lithological composition observed within the MAR region. They are composed of magnesium-rich minerals, and they are formed through the alteration of ultramafic rocks, specifically peridotite, upon exposure and hydration with seawater. Serpentines exhibit a characteristic greenish-grey colour and possess a waxy texture. These minerals are frequently found in regions of hydrothermal activity and fault zones. The presence of serpentines has significant implications for the study of the MAR due to their potential to serve as a setting for hydrothermal vents.

- Dolerites are commonly found in geological formations known as dykes and sills. These are igneous rocks with a fine-grained texture and dark coloration that form due to the rapid cooling and solidification of magma. Dolerites consist of plagioclase feldspar, pyroxene, and olivine minerals and have a high silica content. The value of dolerites lies in their utility for investigating the MAR due to their function as an transitional zone connecting the upper and lower parts of the oceanic crust.

- Gabbros are a type of igneous rock characterised by a coarse-grained texture, commonly occurring in the lower parts of the oceanic crust. They are a result of the gradual cooling and solidification of magma beneath the Earth's surface. These rocks are primarily composed of various minerals including plagioclase feldspar, pyroxene, and olivine. The gabbro rock exhibits a characteristic dotted appearance, featuring black and white colours, and notable mineral grains that are discernible without the aid of magnification. The importance of gabbros in the study of the MAR lies in their representation of the deeper parts of the oceanic crust, thereby facilitating an understanding of the subterranean mechanisms at play.

2.2. Hydrothermal Vent Fields

Hydrothermal vents are geological features that emerge as hot springs on the seabed. These fissures in the ocean floor facilitate the emergence of fluids that are both hot and mineral-rich, which can subsequently reach the Earth's surface. The genesis of these fluids can be attributed to the convective movement of seawater within the Earth's crust, which undergoes thermal alteration due to the presence of underlying magma that serves as a thermal reservoir (Fig 7). The chemical composition of the substance may experience modifications through interactions with adjacent host rocks and their respective compositions. (Fisher et al., 2007; Kelley & Shank, 2010; Puzenat et al., 2021). This alteration and a consequent metamorphism get gradually increased going deeper in the crust. Both effects reflect variability based on the distinct sections of the hydrothermal systems in which the chemical exchange transpires. (Alt, 1995). Thus, distinguishing three main ones: Recharge, reaction, and discharge zones.

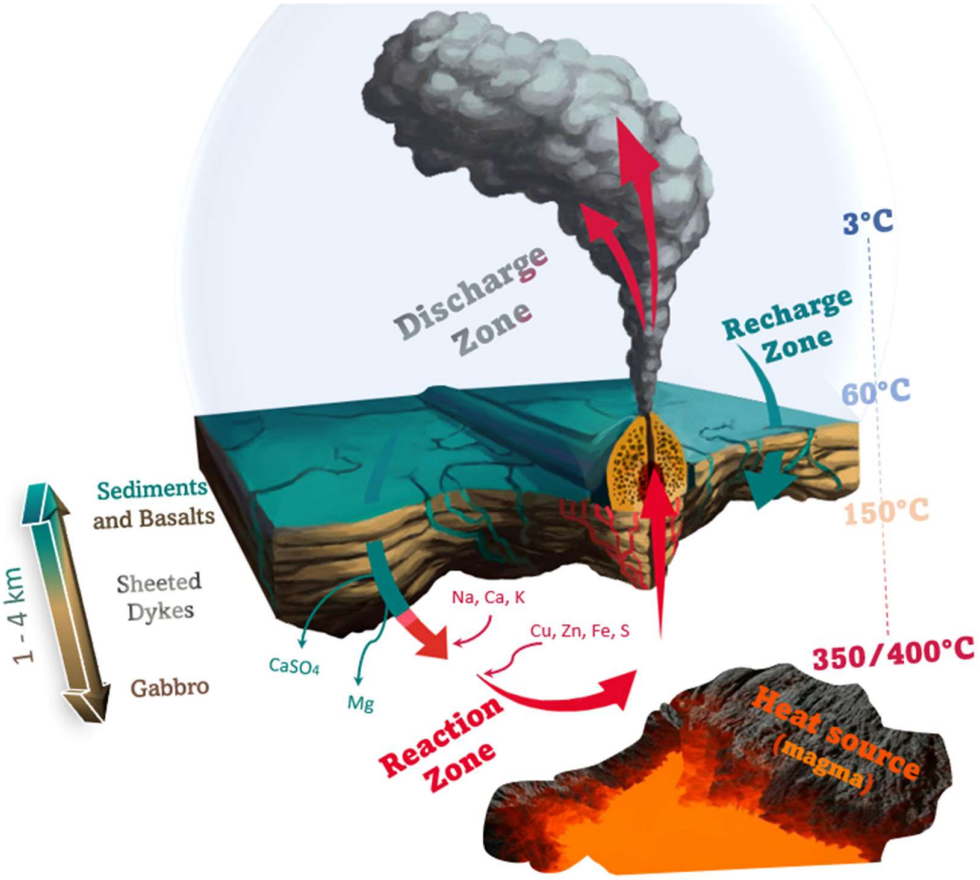

Figure 7. Schematic representation of hydrothermal venting process. Display of different lithologies, temperatures and venting Zones. Modified from picture courtesy of Spencer Sutton.

As seawater penetrates the crust, it reaches elevated temperatures of approximately 400°C, thereby acquiring its distinctive chemical composition and influencing its buoyancy by augmenting it. Subsequently, the fluid rapidly ascends towards the ocean floor. Additionally, as it cools, it causes the creation of sulphide deposits that are abundant in minerals and metals containing Au, Ag, Pb, As, Sb, and Ba, relative to mid-ocean ridges deposits (Tivey, 2007). The demand for these elements is consistently increasing in order to facilitate the development of green technology and ensure the continuity of the intended economic growth. (Hallgren & Hansson, 2021).

Regarding a geological background, hydrothermal venting can vary greatly when it comes to its origin settings (Dover, 1995; Zeng et al., 2020). Vent fields are present in various geological formations such as Mid-Ocean Ridges (MORs) like the Mid-Atlantic Ridge (MAR), back-arc basins (BaBs) such as the Okinawa Trough near Taiwan, island-arcs (IAs) like the Eastern Manus Basin in Papua New Guinea, and hot spots like Strýtan in Iceland.

2.2.1. Hydrothermal Vent Features

The presence of diverse geographical features can lead to the occurrence of multiple basement rocks exhibiting distinct chemical properties, therefore resulting in a range of hydrothermal outputs.

This thesis will focus on the lithologies of MORs rather than looking into the mentioned BaBs or IAs. The area contains volcanic rocks that exhibit abyssal peridotites and other remnants of magma that experienced significant alteration due to exposure to seawater. This is evidenced by the presence of elemental anomalies such as Rb, Ba, Sr, Li, and Pb, which suggest a source originating directly from the Earth's mantle (Langmuir et al., 1997). Based on the available data, it can be determined that the hydrothermal vents produce products such as vent fluids exhibiting a thermal gradient ranging from 66º- 403º C and pH levels that can vary from 2.6 to 10.6 under standard conditions (25ºC and 1 atm). Typically exhibiting elevated levels of H_2S, Fe, and Mn (Zeng et al., 2020).

Historically, the main strategy for identifying and categorising hydrothermal vent fields has been to search for indicators such as chemical footprints or heat anomalies. This is largely due to the extensive knowledge and experience that has been accumulated through the use of these

methodologies (German et al., 2010). Although remote sensing approaches such as the one proposed in this thesis, are gaining popularity due to improvements in technology.

In the domain of geomorphology, an extensive understanding of the geological features present in the hydrothermal vent field is essential for its subsequent categorization.

2.2.1.1. Hydrothermal features at a Bathymetric level

On a larger scale, volcanic landforms have been identified along the MAR or other slow spreading ridges. These landforms are useful for bathymetrical interpretation as they exhibit continuous and identifiable shapes that do not require high resolutions (Palgan, 2017):

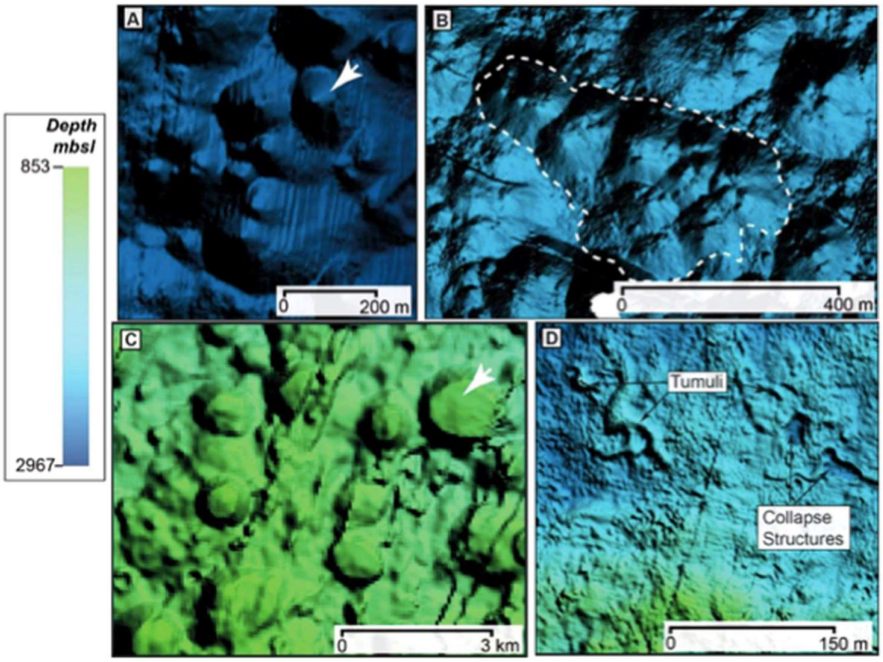

Figure 8. Examples of volcanic landforms distinguished under bathymetric resolutions: A) Volcanic Hummocks. Bathymetry gridded at 50m; B) Hummocky Ridges. AUV Bathymetry of 1m resolution; C) Flat-topped volcanoes. Bathymetry gridded at 35m; D) Flat lava flows (lobate flows) with detailed structures such as hummocks, conical volcanoes (tumulis) and collapse structures. AUV bathymetry of 1 m resolution. (Palgan, 2017)

- Volcanic hummocks represent the most prevalent and small monogenic landform in the MAR, characterised by heights up to 300 metres, steep slopes, and diameters that vary from 50 to 500 metres.

- Hummocky ridges are created through the clustering of multiple volcanic hummocks, resulting in a larger volcanic feature that can be easily identified through bathymetry. They have the potential to reach a length of multiple kilometres, have a width ranging from 100 to 2 kilometres, and achieve an elevation of up to fifty metres above the surrounding seabed.

- Eruptive fissures are a commonly observed site for effusive eruptions, and their formation can be attributed to one of three processes: magmatic intrusions, lithosphere stretching, or thermal contraction. These fissures are characterised by the presence of inflated lobate and pillow lavas. The formation of recognizable wrinkles around them is attributed to the process of folding.

- Flat-topped seamounts can be easily identified in bathymetric datasets. Their circular shape is susceptible to tectonic deformation. These types of volcanoes are commonly referred to as "flat-topped volcanoes" and typically exhibit a flattened summit. They can present a radius of 1-2 kilometres and reach heights of 50-200 metres.

- Axial volcanic ridges are formed through the superposition of the volcanic features previously described. They are the most common features, particularly in the Mid-Atlantic Ridge. Additionally, these distinctive composite volcanoes serve as the principal constructors of the emerging volcanic region.

2.2.1.2.Hydrothermal features at a Mosaic level

To conduct a mosaic analysis at an increased resolution in comparison to the bathymetry, a more detailed classification can be executed. This implies that the volcanic characteristics observed have the potential to meet the criteria for different lava categories. Thus, similar to those seen on land, submerged lava flows display a variety of morphologies.

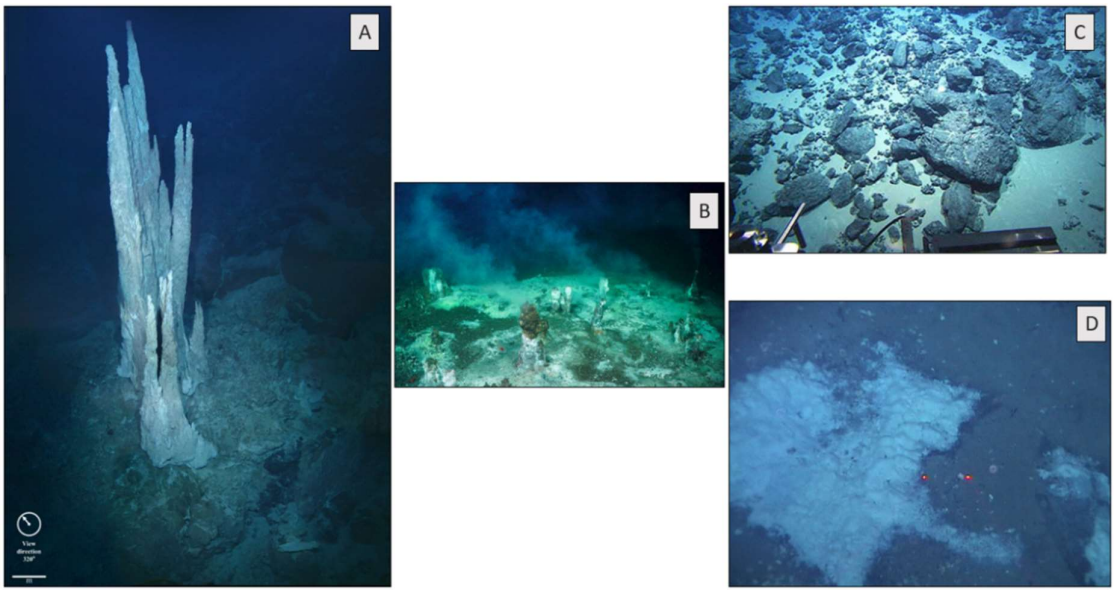

Figure 9. Examples of hydrothermal formations distinguished under mosaic resolutions: A) A group of limestones chimneys at the Lost City Hydrothermal Vent Field at the Mid-Atlantic Ridge. B) Bacterial mats and hydrothermal chimney in the Gulf of California. C) Prominent basement rocks on the steeply sloping side of the Western Massif of Lost City Hydrothermal Vent Field. D) Bacterial mat seen at the Blake Ridge diapir. The two red dots near the center of the image are laser pointers from the sub used to measure the size of a targeted object. These two points are always 10 cm apart. Images courtesy of NOAA agency

The lava morphologies that are commonly observed on the mid-ocean ridges include pillow lavas, lobate flows, and sheet flows. (Dover, 1995; Mitchell, 2018).

In addition to the various classifications of lava, the mosaic in question also features identifiable examples of hydrothermal vent features:

- Bacterial mats are dense layers of microbial communities that form in close proximity to hydrothermal vents. Vent streams often contain particular bacteria that possess the ability to degrade the chemical compounds and minerals present within them. The high reflectance of the object towards artificial light results in its noticeable appearance in the image, due to its bright white shade.

Chimneys and their corresponding shadows are easily discernible. The mineral deposits, mainly made up of metal sulfides, that can be found in the vents' surroundings are used to create these tall, hollow structures. Chimneys can be subclassified as:

- Sulphide edifices are intricate and extensive formations composed of metal sulphides and various minerals that may appear in proximity of hydrothermal vents. These entities have the ability to last for many years, achieving considerable heights.

- The black smokers discharge water that is rich in sulphides and minerals, typically characterised by dark plumes of water that contribute to their distinctive appearance. (The term "smokers" is attributed because of how much they mimic smokestacks from factories.)

- The white smokers emit mineral-rich plumes of water, typically composed of silicon, calcium, and barium. Hydrothermal vents of this type are comparatively infrequent in comparison to black smokers and tend to occur at lower temperatures.

The various vertical structures have been regarded as a unified entity in the categorization process. The structure in question has been referred to as "chimney." As shown in Fig. 9 (A), the vertical nature of the structure makes it more challenging to discern through superficial mapping techniques, as it blends easily with other features. Thus, the small bathymetric alterations play a significant role. For this reason, it is strongly recommended that a high-resolution bathymetry is employed to detect even the slightest variations in the topography of the seabed.

- The basement rocks (Snook et al., 2018) and mounds of spire fragments and hydrothermal sediments are highly significant for mining purposes due to their inactive nature, characterised by low temperatures and the absence of any living ecosystems in the immediate area. During the process of mosaic analysis, they present a substantial surface of the sea floor.

2.2.2. Loki's Castle Hydrothermal Vent Field

The location of the LCHVF is situated at the juncture of the Mohns Ridge segment's northward turn into the Knipovich Ridge, more precisely at coordinates 73°30′N and 8°E. This northern region of the MAR is called The Mid-Ocean Ridge (AMOR) (Pedersen et al., 2010).

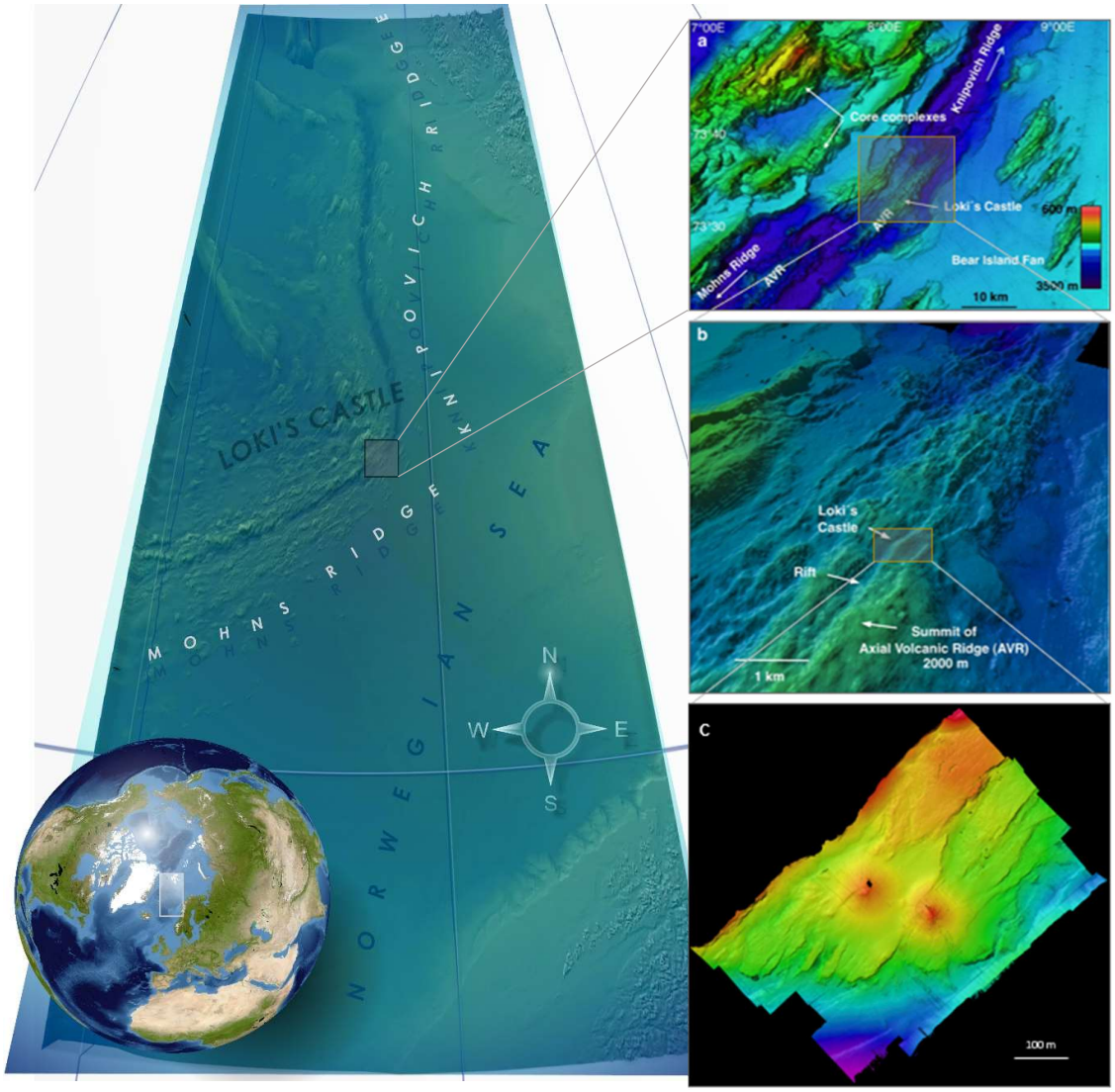

Figure 10. Bathymetrical augmentation from (a) the Axial Volcanic Ridge (AVR), with an expanded perspective of the AVR as observed from a southern oblique viewpoint (b). The LCHVF emerges at the centre of the crest, while an inset of the hydrothermal vent showcases the Eastern and Western mound subdivisions, along with their corresponding vents (c). Bathymetry maps from (Pedersen et al., 2010)

The LCHVF is situated at a depth of roughly 2400 metres. The AMOR is classified as a ultraslow-spreading ridge, spreading at a rate of approximately 6-15 mm/yr. The geological composition of the area surrounding the vent field is predominantly constituted of basaltic

rocks, with a minor presence of gabbroic and ultramafic rocks in the underlying strata.
The vent field is named after the Loki's Castle vent, which is the largest of the vent sites and is located at the top of a volcanic edifice. The edifice is composed of a mixture of basaltic and rhyolitic rocks, which are thought to have been formed by volcanic activity related to the Mid-Ocean Ridge (Snook et al., 2018).

At the Loki's Castle Hydrothermal Vent Field there is a discharge of black smoker fluids emanating from chimneys that can reach heights of up to 13 metres, numbering four in total. The chimneys are located on two hydrothermal mounds, with an approximate distance of 150 metres between them (Fig. 10 (c)). These mounds are estimated to have a height of 20-30 metres and a width of 150-200 metres (Jaeschke et al., 2012).

The Eastern mound, 150m east of the western mound, and has the same size and composition. The eastern mound contains only one hydrothermal vent at the top, called João, while the western mound has three. The mound's most prominent characteristic is the high-temperature, focussed vent (João), yet bacterial mats cover much of it, indicating a significant fraction of diffuse outflow.
The Western mound has a diameter of 150-200m and is 20-30m tall. The mound contains mostly pyrite, sphalerite, and pyrrhotite. Three high-temperature (>300°C) black smoker vents are evenly distributed from northwest to southeast on the mound. The northwest vent, Sleepy, is the least active of the three smokers. Menorah and Camel are the middle and southeast vents, respectively. Menorah and Camel have multiple chimneys, whereas Sleepy has one rounded chimney (Pedersen et al., 2010).

The Loki's Castle Hydrothermal Vent Field is considered a suitable location for the finding of sulphide mineral deposits with regards to its potential mineral resources. These deposits exhibit elevated levels of metallic elements, including copper, zinc, and gold, that are of significant economic importance (Koschinsky et al., 2018). However, the exploration and exploitation of these resources requires careful consideration of the potential environmental impacts and the sustainability of such activities.

The Loki's Castle Hydrothermal Vent Field is under Norwegian jurisdiction (Fig. 28) as it falls within Norway's Exclusive Economic Zone. Starting this year, the Norwegian government will grant licences exclusively for scientific research and exploration purposes in the region to private enterprises. The assumed extinct site known as "Mohns Treasure" is the target location for their mission (Directorate, 2023).

2.2.3. Lucky Strike Hydrothermal Vent Field

The LSHVF is situated on the southern section of the Mid-Atlantic Ridge, more precisely at 37°17′ N and 32°16′ W. It lies approximately 400 km southwest from the Azores archipelago, at a depth of around 1500 meters and with a slow spreading rate of roughly 22mm/year (Humphris et al., 2002).

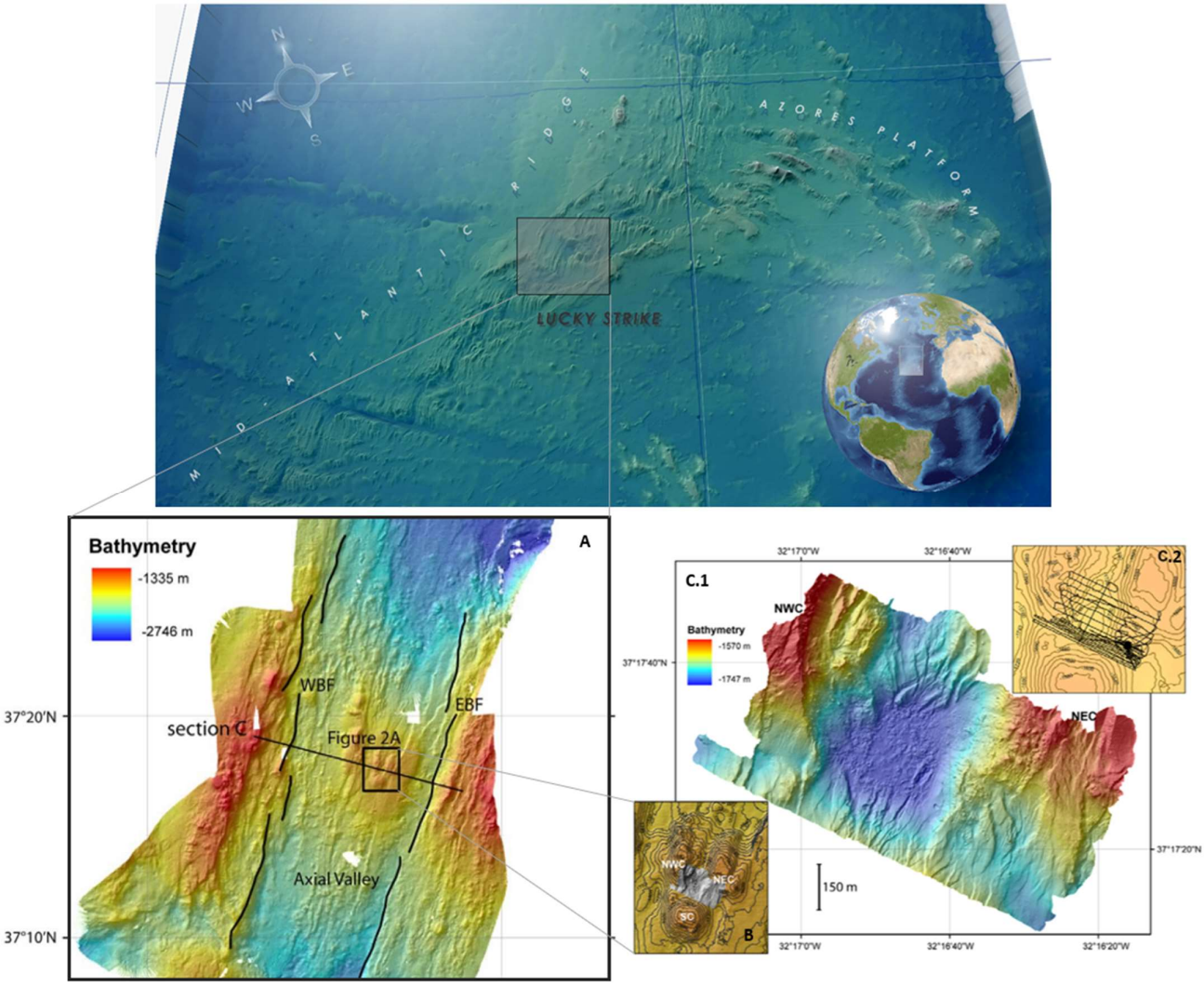

Figure 11. Bathymetrical augmentation of the Lucky Strike Hydrothermal Vent Field from (A) the Lucky Strike segment from shipboard multibeam data highlighting the summit of the central volcano (box Figure 2a). Lines show locations of the main axial valley bounding faults (WBF: west bounding faults and EBF: east bounding faults). (B) Map containing the shaded high-resolution LSHVF bathymetry (C.1), surrounded by the three volcanic cones NWC: Northwest volcanic Cone, NEC: Northeast volcanic cone and SC: South volcanic Cone. (C.2) Tracks of the ROV Victor. Bathymetry maps from (Ondréas et al., 2009).

The area is characterized by a high degree of tectonic activity, with frequent earthquakes and volcanic eruptions along most of the sea floor in this segment, south of the Azores platform. Meaning that the Azores hot spot has a significant impact on this system (Kelley & Shank,

2010). At the centre of the Lucky Strike segment, on the summit of a noticeable volcano, the Lucky Strike hydrothermal vent field covers an area of over 1 km2 (Fig.11, C.1). At Lucky Strike, venting sites include ridges with pool temperatures above 200°C, black smokers with fluids as hot as 333°C, and chimneys releasing diffuse fluids with lower temperatures. Hydrothermal venting occurs in four main regions, each of which contains several chimneys, some of which are well-known, such as Sintra, the Tour Eiffel, and Montsegur (Ondréas et al., 2009). These Lucky Strike vents are situated in the vicinity of an even stretch of smooth lava and remarkable columnar formations, which have been considered as the remnants of a fossil lava lake. The identification of the lava lake below the Lucky Strike volcano implies the presence or recent activity of a subterranean magma chamber within the Earth's crust. This statement suggests that the composition of the hydrothermal vent consists of basaltic rocks, which are formed through the process of lava cooling and solidifying (Langmuir et al., 1997).

The hydrothermal vents situated towards the southern and western regions of the lava lake are constructed on a unique stratified basaltic breccia formation, which is occasionally cemented by silica. This formation appears in the form of a slab-like material, measuring up to one metre in thickness. It is believed to be formed due to a localised explosive volcanic activity. Subsequently, it was cemented by silica that precipitated from the combination of hydrothermal fluids and seawater (Humphris et al., 2002; Ondréas et al., 2009).

The LSHVF and its resources are located in the Marine Park of Azores (Menini & Van Dover, 2019) . The site includes distinct regions that encompass diverse marine environments, such as seamounts, banks, submerged islands, and hydrothermal vents. The Portuguese EEZ covers two hydrothermal vent fields (Fig. 28), including Lucky Strike and also Menez Gwen, which are situated within the Park. These vent fields are defined by their significant depth, exceeding 500 metres, and have been declared as Marine Natural Reserves. As such, all economic activities, such as deep-water fishing and resource exploitation, are forbidden within these reserves.

2.3. Hydrothermal Vents as potential mining sites.

Known as massive sulfides or polymetallic sulfides, the minerals formed as a result of the hydrothermal vents activity are key factors for the so-called Green Transition (Church & Crawford, 2020). In which rare metals are used for high-tech tools and objects such as batteries for transportation, electronic devices or for storing solar and wind energy.

For the past forty years, deep-sea mining (DSM) activities have seen ups and downs within its funding and evolution. DSM experienced a considerable boost after the end of the decolonization, in efforts to close the inequality gap between rich and poor countries. As discussed in (Hallgren & Hansson, 2021), minerals found on the deep seabed, ones that lie beyond any countries jurisdiction, belong to nobody and everybody, i.e., they are a common good (Fig. 3). Therefore, the international authorities which deal with its regulation have the duty to create and follow a system that is equitable and fair. With this purpose, the ISA was created in 1994, a UN body in charge of ensuring the integrity of the marine environment (Blanchard et al., 2023; Miller et al., 2018).

As of now, there has not been an issue of mining licences. The ISA operates by granting approval to a plan of work (PoW) for the exploitation of each mineral resource . On June 25th, 2021, the Republic of Nauru initiated the implementation of the Law of the Sea by formally requesting the ISA Council to adopt regulations within a two-year timeframe that would facilitate the approval of the PoW for exploitation.

In contrast, as a measure of precaution, the European Union Parliament voted for a moratorium of exploitation activities in the year 2018, and has reaffirmed the same position in 2021. Regardless of its limited impact on the Member States, the Council's elected representatives did not formally suggest a moratorium. Instead, they focused their efforts on enhancing the draft's existing environmental regulations (Ardito & Rovere, 2022).

There are still numerous uncertainties which can cause severe or even permanent damage to an ecosystem during the extraction process, that humanity barely understands yet. There is still a lot of research ongoing, and is needed to wait and see what it uncovers, or else most of the ongoing initiatives may just turn hazardous.

This thesis therefore aims to point out the strong relationship between new methods of underwater exploration and the conservation of the marine environment as intended by the UN.

3. Theoretical Background

3.1. Development of deep-sea mapping techniques

Egyptians are thought to have been the first to try to figure out what was beneath the water's surface. They would post a person at the bow of the boat, holding a long pole into the water, tracing the submerged bottom in order to warn if any obstacle would hit the hull (Wölfl et al., 2019). More than a century ago, the little information available was obtained by using rudimentary technics such as dropping a lead weight tied to a line over the edge of a boat and measuring the length to the bottom. Within a short amount of time, these technologies evolved into single beam echo-sounders, which acted as a bridge to the multibeam surveying that is used nowadays.

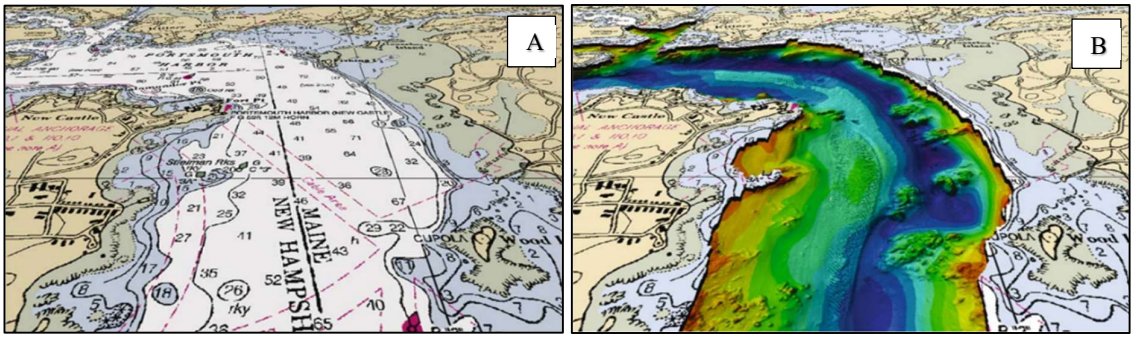

Figure 12. Single beam sonar data (A), which is made up of random soundings and curves interpolated from spare soundings. Comparison to multibeam sonar data (B), which represents a much more detailed bathymetric description. (Mayer, 2006)

To observe any region of the ocean more precisely, researchers employ echo-sounding technology rather than satellites, typically used for on-land surveys, because of the increased resolution. Echo-sounding is the use of sonar technology, short for SOund NAvigation and Ranging, as a tool (Eason et al., 2016) typically for determining water depth (bathymetry) through sound waves. It functions by releasing the acoustic waves into water and measuring the time interval between pulse emission and return; the resulting duration of "flight", considering simultaneously the speed of sound in water, allows scientist to estimate the distance between sonar and target.

Onboard sonar systems nowadays can image the ocean floor at a resolution of around 100 metres across a thin strip below the ship (Fig. 12). These highly precise maps have currently only covered the previously mentioned percentage of 18%, an area roughly the size of Africa (Mayer, 2006). Moreover, when trying to detect anything only a few metres in size on the ocean

floor, such as the mineral spires of hydrothermal vents analysed in this study, sonar equipment must be brought exceptionally close to the seabed utilising underwater vehicles or towed devices. At this level, sonar has mapped less than 0.05% of the global ocean floor to that maximum degree of detail, an area roughly the size of Ireland. Thus, in order to add more information to obtain a more complete dataset, the combination of bathymetric and photomosaic's surveys is applied.

Autonomous Underwater Vehicles (AUVs) and Remotely Operated Vehicles (ROVs) are responsible for collecting photographic and multibeam data with higher resolution than the ships themselves since they can dive with almost no restriction (Fig 13), with the most advanced vehicles reaching almost the deepest point in the ocean (11000 mbsl). While ROVs are controlled remotely and powered from a vessel, AUVs operate autonomously, with only their own power supply limiting their range.

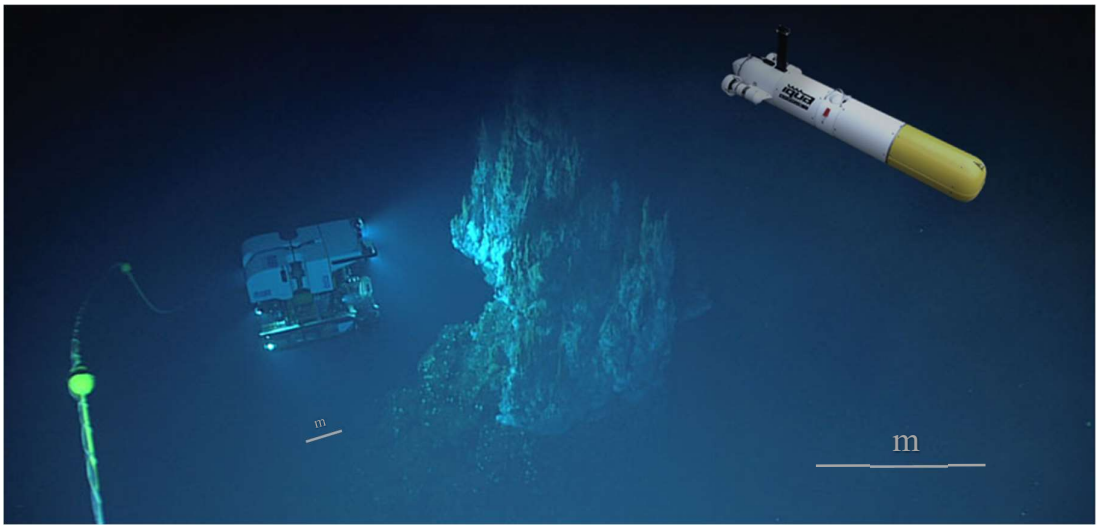

Figure 13. Interpretative collage of underwater vehicles ROV Deep Discover (left) and AUV Sparus II (right). Pictures courtesy of NOAA and IQUA Robotics Spain respectively.

The establishment of these near-bottom mapping techniques is still impractical for surveying broad areas, due in part to their low speeds in comparison to ships (Wölfl et al., 2019). In addition, they are not yet capable of declaring ship-based surveys obsolete, as the positioning detail of AUVs remains restricted, and it is still required to roughly grasp the bathymetry of a region before a submersible can be dived down to the seafloor autonomously.

Generally, the volcanic features, with all their associated intricacies, have been identified visually on a photomosaic. A photomosaic is an aggregation of images generated by the

submergible vehicles, which captures individual pictures within visual range of the seafloor, at ~10 m. These individual images are then put together into a mosaic to create a clear visual of the seabed area, resulting in resolutioins as good as 1cm. In addition, AUVs can map multibeam surveys ~50 m off-bottom (Keohane & White, 2022), which simultaneously increases the speed of data collection and, thus, the potential area of study. While these methods are effective, they can be tedious, subjective, time-consuming and expensive, and are limited by the resolution and range of the sonar equipment. To this date, the vast ocean floor has only been analysed manually, and studies have been very selective and focused solely along high-interest areas due to the extraordinarily arduous nature of this task.

3.1.1. Manual Deep-sea image interpretation.

Mapping the sea floor is an important task for understanding the ocean's geological and biological characteristics. Advanced imaging techniques, such as sonar, have facilitated the acquisition of extensive data related to the submerged environment (Fig. 12). However, the intricacy of the data often requires the use of advanced software tools to extract significant information from it.

Image interpretation is a vital process for the extraction of information from visual data. It involves analysing visual information to identify patterns, features, and objects, and then drawing meaningful conclusions from that information. The analysis of visual representations has an extensive and rich history, with early examples dating back to the 19th century, during which cartography and aerial photography were used to interpret geographic information (Cohen, 2000). Following to that period, the progression of technology has facilitated the acquisition and analysis of images with progressively improved precision and intricacy, making it an indispensable instrument for numerous disciplines, such as marine science.

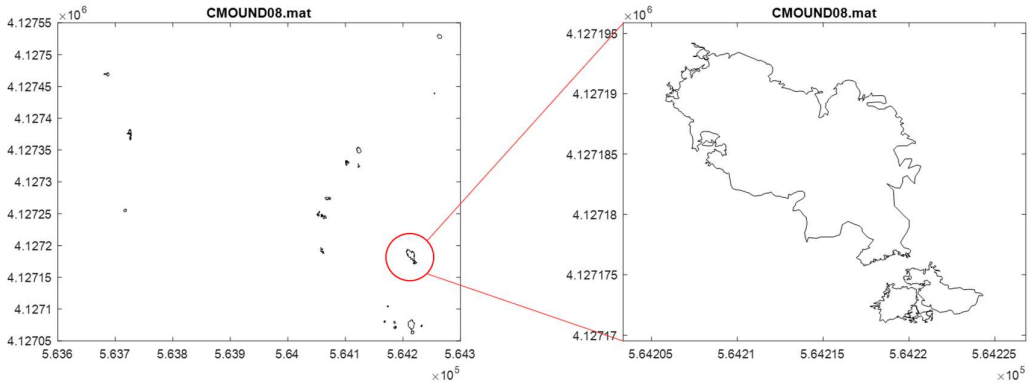

Figure 14. Mound structures from LSHVF plotted manually using Matlab.

Traditionally, deep-sea landforms have been delineated and categorised through subjective interpretation, whereby geologists relied on their prior experiences to identify and classify features, which were subsequently reviewed and revised by other geologists.

The techniques employed were found to be laborious and evidently reliant on personal judgement, given that the accuracy of the specialist categorizations was restricted to a relatively limited number of samples (Fig. 14) and evaluators (Mayer, 2006). In the field of biology, a comparable scenario would arise as the creation of a repository capable of accommodating all the species encountered during the course of study, in which some are not even static. This process necessitates as well great attention to detail towards potential counting inaccuracies. Leading again to an higher susceptibility to human errors during the process of interpretation.

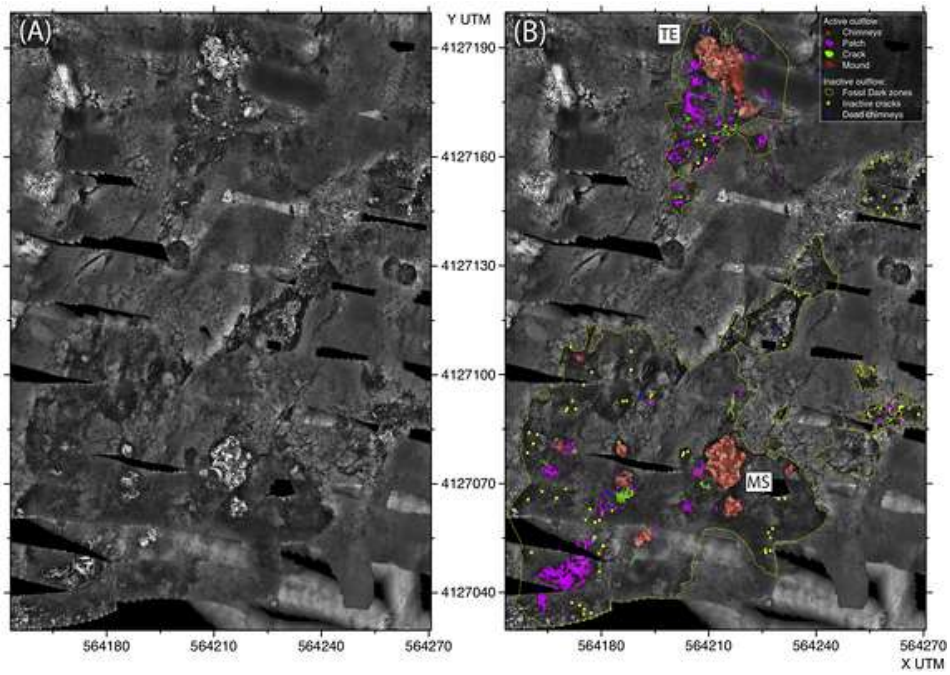

Figure 15. Image mosaic analysis with in situ observations reveal a detail classification of the south-eastern half of the Lucky Strike hydrothermal field (A) and manually identified hydrothermal structures, both active and inactive (B). (Barreyre et al., 2012)

Figure 15, along with other examples displayed in the publications cited hereafter, serve as illustrations obtained so far from manually characterised underwater geological features. (Barreyre et al., 2012; Gini et al., 2021; Puzenat et al., 2021; Somoza et al., 2021)

This raises the issue of how and by whom the determination of what is considered right and wrong. Simultaneously, it presents a potential resolution by enabling artificial intelligence an opportunity to generate classifications that are as objective as feasible, based in objective parameters.

3.1.2. Deep-sea image interpretation automation

As more and more expeditions are carried out every year, the amount of data available is constantly increasing. As a result, there have been a number of significant efforts in recent years to develop automated methods for the interpretation of deep-sea imagery (Ricard Prados, 2012). This requires the development of scalable algorithms that can handle the large amounts of data generated by modern deep sea imaging systems, so it can classify and identify the different types of volcanic seafloor features and marine life (Sonogashira et al., 2020). Hence, machine learning (ML), a type of artificial intelligence, has been essential for the automation. It enables computers to learn from data, developing algorithms that can analyse and make predictions or decisions based on patterns in the data (Ditria et al., 2022). There are several types of ML, including supervised learning, unsupervised learning and reinforcement learning. In addition to these, it is also worth just mentioning the efforts to use other computer vision techniques, such as stereo reconstruction (Ye, 2022), to create detailed 3D models of the seafloor. Or the magnetic exploration (Guo et al., 2023) based on accurate and autonomous interpretation of anomalies in the geomagnetic fields of certain ore resources such as iron, ore, lead-zinc ore and copper ore.

While ML and AI have shown considerable potential for mapping landforms in the deep sea over traditional techniques, there are still several research questions that remain unanswered. While some recent publications have already made some significant findings with regards to seafloor mapping together with AI, as evidenced by the work of (Jiang & Zhu, 2022; Keohane & White, 2022; Sonogashira et al., 2020; Ye, 2022). The main task ahead is the need to develop more efficient algorithms. These ML models require improvement in their ability to learn from unlabelled data (Ditria et al., 2022) in a quicker and more accurate way.

In addition to improvements to the mapping technologies themselves, there are still other areas where further research is needed to improve the automated interpretation of deep-sea imagery. One important and necessary leap is the need for new methods of handling data from multiple types of sensors like cameras, sonar, and lidar, that could provide complementary information about the environment (Miller et al., 2018) and at the same time, its protection.

This novel technology has been used by the Department of Earth Science at UiB. Which now possesses data related to multiple scientific initiatives that have primarily focused on the Mid-Atlantic region in the past few decades. This thesis gets then, significant importance in defining the appropriate mapping method of this geological setting, utilising an interdisciplinary approach with the latest improvements in technology.

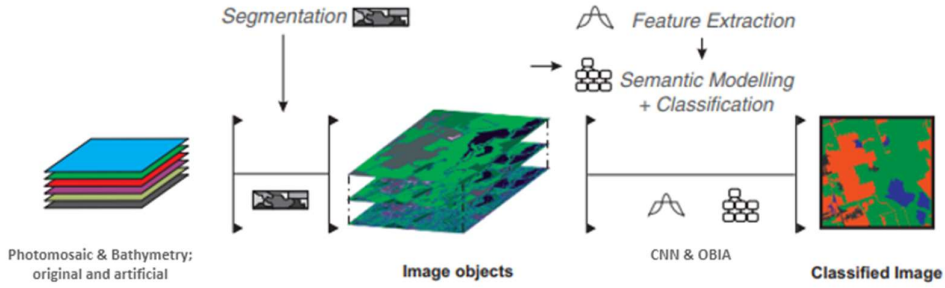

Figure 16. Machine Learning workflow followed in this thesis. Modified from (Gupta & Bhadauria, 2014)

One such tool is eCognition, a software application that has been specifically developed for the purpose of advanced image analysis and interpretation. The main advantage of this platform lies in its powerful segmentation algorithms and its ability to perform hierarchical, cross-linked modelling and classification. (Nussbaum et al., 2008). The advanced ML techniques employed by eCognition facilitate its robust image analysis capabilities. The implementation of artificial intelligence techniques enables computer systems to acquire knowledge from data sets, without the need for explicit programming.

Within the field of image analysis, ML algorithms get trained using extensive datasets of labelled images, which allows them to identify patterns in new images.
Deep learning is a highly effective ML technique that is commonly employed in the field of image analysis. This methodology utilises neural networks to detect patterns in visual data.
Once all the data is collected, the methods that follow can be divided in three sections (Fig. 16): first step is pre-processing the imagery for an effective management in the post-processing software, eCognition. Following that, the primary goal is to discover the most accurate output or heatmap that clearly represents a differentiation between the sought features. One of the preferred techniques has been supervised learning algorithms.

Convolutional Neural Networks (CNNs) and Object-Based Image Analysis (OBIA) are two methods with strong potential for the image classification tasks (Fig 16), notably because they have already been shown to be effective at identifying and classifying different types of

landforms from satellite and aerial imagery (Robson et al., 2020). An introduction to these two methods is followed. Moreover, it will get further explained in the methodological definitions.

CNNs

Convolutional Neural Networks refer to computational models that are designed inspired on the structural and functional characteristics of the human brain. They composed of multiple layers of interconnected nodes, commonly referred to as "neurons" which collaborate to recognise and discern patterns that are present within the data. (Gupta & Bhadauria, 2014).

Once trained, deep learning algorithms are particularly useful in the domain of underwater imaging, due to the ability to gather enormous quantities of data that is collected during a single cruise. Manual analysis of such data is both time-consuming and prone to errors, thereby demonstrating the value of deep learning algorithms in this context. As an illustration, a deep learning algorithm might receive training on a dataset which includes images capturing underwater ridges, with the aim of acquiring the ability to recognise these same characteristics in novel images.

OBIA

Object-Based Image Analysis is a methodology that offers an alternative to pixel-based approaches by utilising image objects as the fundamental analysis unit, rather than individual pixels (Robson et al., 2015). The objective is to assess more complicated classes that are characterised by spatial and hierarchical associations both within and throughout the classification process (Fig. 16).

OBIA is characterised by its focus on the segmentation of remote sensing imagery into meaningful image-objects, and the subsequent analysis of their properties using a range of spectral and spatial measurements (Hossain & Chen, 2019).The primary objective of this approach in this thesis is to offer a technique for examining high-spatial resolution imagery through the application of spectral, spatial, textural, and topological underwater-attributes whereas pixel-based methods are frequently restricted to spectral indices.

The results obtained are crucial in comprehending the complex geological processes occurring beneath the water surface. Deep learning algorithms can be employed by researchers to detect features of interest, such as hydrothermal vents, and subsequently apply this information to better generate cartographic representations of the seabed.

4. Data

The following chapter explores the ways to gather data utilised in this thesis, as well as the strategy for its management. The chapter can be divided in two distinct sections that follow one another: Types of data and how the datasets were acquired and pre-processed.

The two primary categories into which these datasets have been classified based on their characteristics are photomosaics and bathymetry imageries.

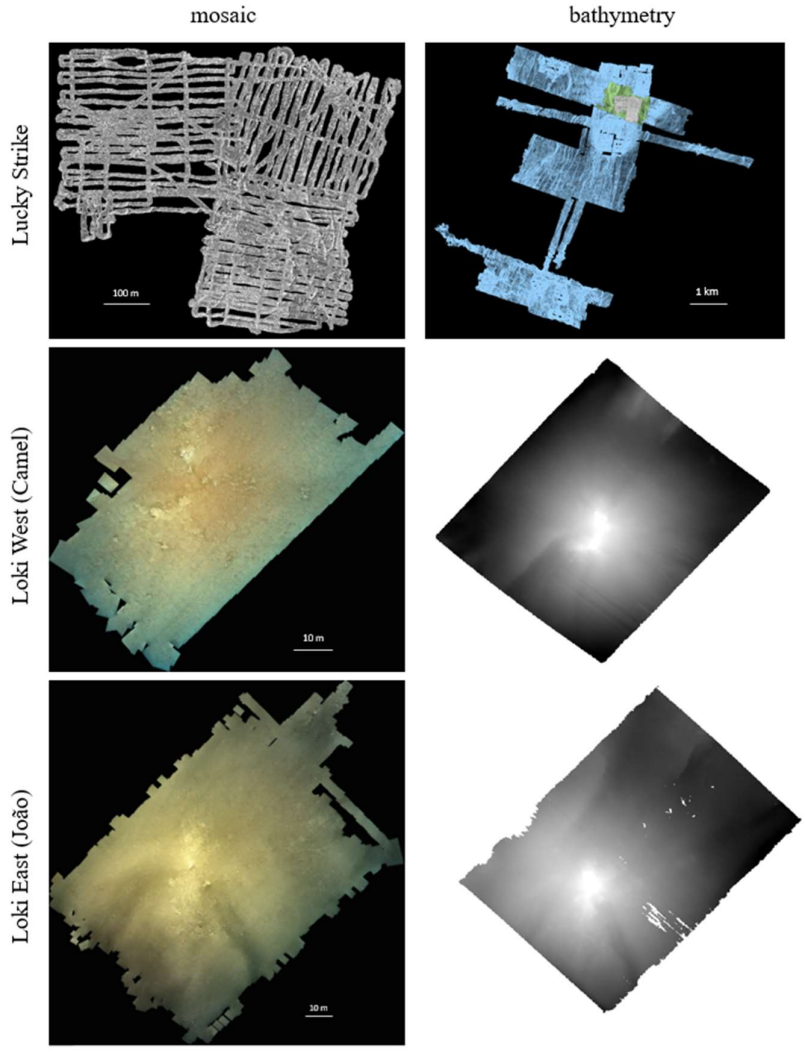

Figure 17. Examples of the raw datasets utilised.

The entire set of the dataset utilised in this study were provided by my co-supervisor, Thibaut Barreyre, whose research interests include Deep-Sea Instrumentation and Exploration. When downloaded, all geospatial data was set to their specific coordinate reference system (CRS): ETRS 1989 UTM Zone 32N for Loki's Castle and WGS 1984 UTM Zone 25N for the Lucky Strike Hydrothermal Vent Field.

4.1. Photomosaic

The photomosaic is a composite image created by merging multiple photographs captured using a vertically mounted, down-looking electronic black-and-white still camera on the ROV utilised for conducting the surveys. In order to ensure a uniform and proportional merging, is needed to maintain a constant distant from the sea floor, that is an altitude ranging from 5 to 10 m above the seafloor. Moreover, keeping a reduced cruising speed for the ROV contributes the image to seem steady.

As an illustration, the mosaic MoMAR08 is utilised to cover the LSHVF, affecting an area of 267179 m^2. It is composed by 21262 images that took 101 hours of survey to make. Finishing with a photomosaic of 1 cm resolution.

To overcome this characterisation. During the cruises like the one previously mentioned, a photographical survey is planned. The raw images are taken while a vehicle that is controlled remotely from the research vessel traverses the seafloor surface containing the hydrothermal field. (Barreyre et al., 2012; Escartín et al., 2008; Humphris et al., 2002).

Two photomosaics as classified in (Table 1): ROV_30 and ROV_31 illustrate respectively Loki East (João, barite field, oasis) and Loki West (Sleepy, Menorah, Camel).

The previously mentioned vehicles used for this task went by the names of VICTOR6000 for Lucky Strike and Ægir 6000 for Loki's Castle.

To build the mosaic, as explained from (Ricard Prados, 2012). First, captured raw images are pre-processed to, among other things, adjust the overall brightness across photos. Secondly, equalize unequal illumination from the lighting system and imaging geometry, and finally rectify the optical geometric distortion caused by the camera lenses.

To create a navigation-based mosaic using vehicle navigation (location, altitude, direction, pitch, and roll), pre-processed photos were scaled, rotated, and projected originally, and a second time to adjust minor details and make them overlap as this thesis requires.

Among other instruments needed for measure the temperature, pH and other geochemical parameters (Mayer, 2006), the remote operated vehicle or ROV is equipped with lighting apparatus specifically created for low-light conditions, such as strobe lights.

4.2. Bathymetry

As its Greek-origin etymology reflects, bathymetry is the study of the topography of the ocean floor, which includes the measurement of the ocean's depths and the mapping of the features on the seafloor. To do so, bathymetry, in combination with sonar imaging, is generally utilised to identify volcanic features producing those characteristic colourful maps, where generally red is used to show shallow depths and blue or purple for deeper depths.

The main instrument used in these vehicles is the SONAR. This thesis employs various sonar techniques, including those commonly referred to as (Eason et al., 2016; Escartin et al., 2021):

- Multibeam surveying: Using multiple sonar beams to create a detailed 3D map of the seafloor. It works by emitting sound waves from a ship or a ROV and measuring the time it takes for the sound waves to bounce back, thus analysing the time and intensity of the reflected sound waves.

- Side-scan sonar: A category of active sonar system that is installed on the hull of a ship or mounted to another platform, such as a towfish. As the ship moves, the transducer array sends out signals on both sides, sweeping the seafloor like a flashlight's fan-shaped beam. Side-scans look in straight lines at uniform speeds, allowing the ship to record the ocean floor as it moves. Depending on the survey goals, the towfish will record data at different sound frequencies: a lower frequency (50 kilohertz (kHz) -100 kHz) can cover broad swaths of the seafloor at low image resolution. Higher-frequency pulses (500 kHz to 1 megahertz) record smaller but more detailed areas.

As a result, because side-scan sonar cannot measure bathymetry, it is employed in conjunction with depth-measuring equipment such as multibeam sonar. This available near-bottom multibeam bathymetry (gridded at 40m) presents nominal horizontal resolutions of 0.4m and 1.5m (Barreyre et al., 2012).

Regarding these datasets, the navigation and processing of imagery and multibeam data were done independently. Therefore, it is worth to remember that these datasets show relative offsets of less than 10 m for well-known sites.

4.3. Data Collection

Since 1976, cruise expeditions to specific areas have taken place systematically trying to generate higher resolution maps over the southern edge of the Azores platform in the Mid-Atlantic Ridge (Brundage & Patterson, 1976). In 1992, the FAZAR cruise found the Lucky Strike Hydrothermal Vent Field (LSHVF) (Langmuir et al., 1997) which now serves as the study area for this thesis. Thereafter, several expeditions have improved the quality of the dataset that the scientific community have been working with. And ever since, recent expeditions such as MoMARETO and Graviluck, 2006; MoMAR, 2008; Bathyluck, 2009; MoMARSAT 2010 and 2011 have been constantly updating the dataset (Escartin J., 2015; Keohane & White, 2022).

With regards to the acquisition of bathymetric data. The Lucky Strike ridge section along the Mid-Atlantic Ridge was surveyed using multibeam near-bottom bathymetry. The bathymetry data were collected during surveys with the AUV Asterx and the ROV Victor6000 on three different cruises (MOMARETO 2006, MOMAR'08-Leg1, and BATHYLUCK'09) (Gini et al., 2021). The dataset contains a central grid (LuckyStrike_microbathymetry_Centre) that gathers data from several AUV and ROV dives, and where original bathymetry grids for each dive have been manually merged into a single grid, using other datasets for geographical reference (Escartin et al., 2021).

On the other hand, in 2008, Loki's Castle was first discovered. This hydrothermal vent system was recorded thanks to the research cruises conducted by the K.G. Jebsen centre for Deep Sea Research aboard R/V G.O. Sars consecutively during the summers from 2017 to 2020. The aim of these cruises was mapping, among other studies , the hydrothermal formations along the Arctic Mid-Ocean Ridge (AMOR) (Rikter-Svendsen, 2020).

LCHVF has been covered by three surveys (table 1): one for the eastern mound and barite field (survey #1), one for the western mound and related vents (survey #2), and one for the oasis' fault scarp. After the images have been processed, a total of two photomosaics (ROV30 & ROV31) were produced, representing respectively Loki East (João, barite field & oasis) and Loki West.

Table 1. Data sources and formats utilised for the classification analysis.

Dataset	Source	Cruise	Date	Depth	Vehicle	Mosaic Resolution (m) Grid resolution Bathymetry (m)
MoMAR08	Photomosaic	MOMAR'08 Leg 1	2008	~1500	ROV VICTOR6000	0.01
Bathyluck	Bathymetry	Bathyluck'09	2009	~1500	ROV VICTOR6000	1
Momareto_UTM	Bathymetry	MOMARETO 2006	2006	~1500	ROV VICTOR6000	0.5
LuckyStrike_microbathymetry_Centre	Bathymetry	Bathyluck'09 MOMAR'08-Leg 1 MOMARETO 2006	2021	~1500	ROV VICTOR6000 AUV AsterX	1
Loki East João, Barite Field, Oasis	Photomosaic	CDeepSea18	2018	~2400	Bathysaurus XL ROV30	0.01
Loki West Sleepy, Menorah, Camel	Photomosaic	CDeepSea18	2018	~2400	Bathysaurus XL ROV31	0.01
GS17 Loki Castle, Barite Field	Bathymetry	unidentified	unidentified	~2400	Ægir 6000 ROV01	0.01
GS18 João, Camel	Bathymetry	unidentified	unidentified	~2400	Ægir 6000 ROV02	0.01

5. Methodology

The current chapter has been split into two separate sections. The first section of the paper centres on defining the various steps required to overcome the categorization. The latter section indicates the different parameters employed in every stage (Fig. 16) of the previously explained methodology.

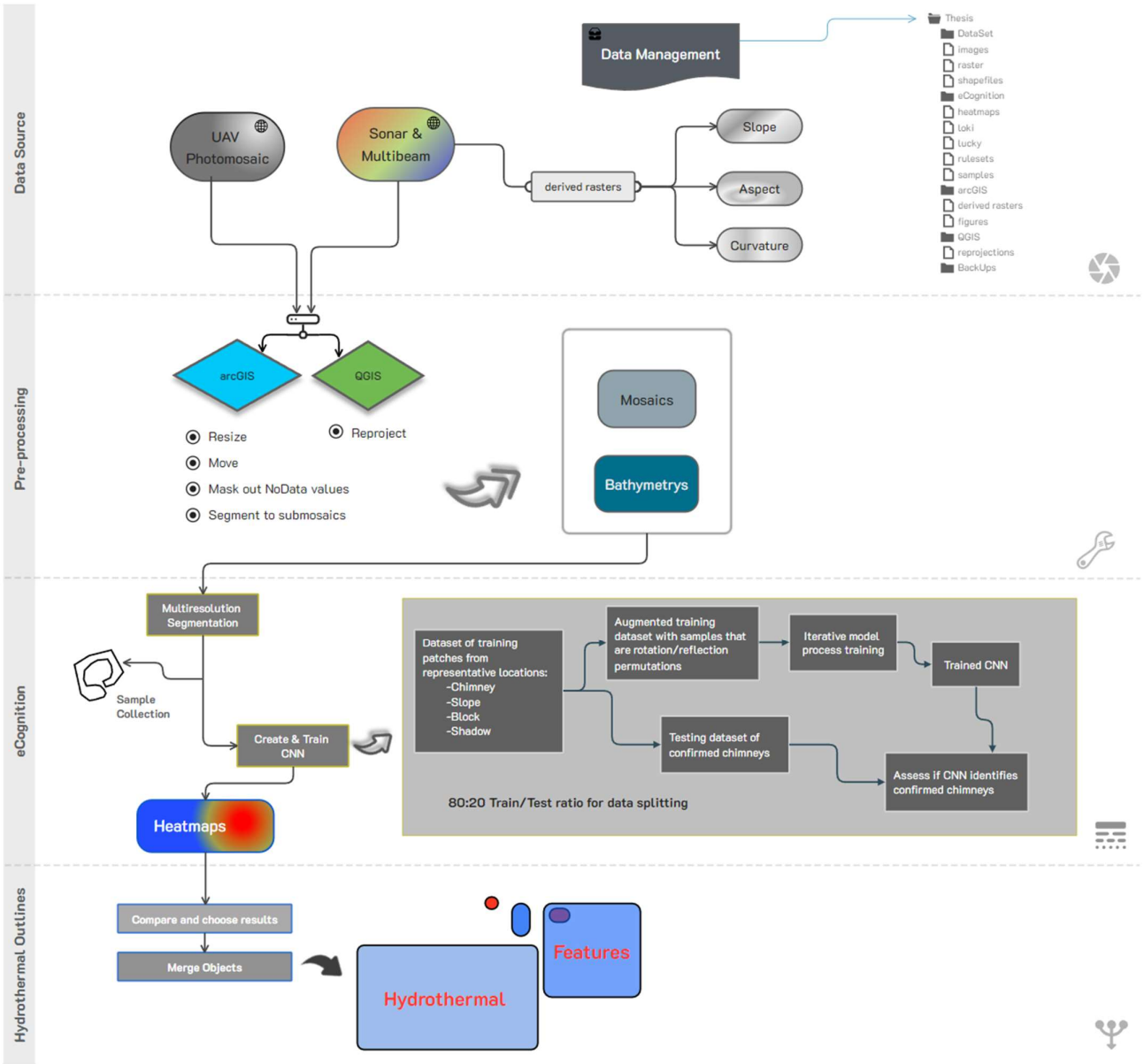

Figure 18. Methodology workflow chart

The softwares that I have utilized and have been successful to use during these steps are eCognition software Developer 10.2 (its CNN workflow is based on Google TensorFlow API), ArcGIS Pro 3.0.2, QGIS 3.28 Firenze and CATALYST Professional Version 2222.0.8

5.1. Methodological processes

5.1.1. Pre-Processing

In general, the efficacy of a deep learning approach tends to increase with the quantity of input samples provided. Acquiring bathymetric images in quantities equivalent to the volume of satellite imagery in on-land classifications presents a challenge in this case, given the limited availability of significant features even across extensively mapped regions. Hence, it is feasible to derive diverse data for a given image or raster through the technique of derivation, such as looking at the slope, aspect, or curvature of the terrain. (Keohane & White, 2022; Sonogashira et al., 2020). The main idea behind producing additions is to virtually increase a larger set of samples by implementing diverse modifications on the pre-existing samples (Fig. 20), as well as standardise the datasets so they are suitable for CNN processing. To achieve this objective, the "Slope, Aspect, Curvature" processing tool in QGIS is utilised on the Loki's Castle's subsets of the original bathymetry data at the locations of Camel, Joao. To generate the corresponding derived rasters possessing such attributes. The Lucky Strike's bathymetric raster, namely LuckyStrike_microbathymetry_Centre, has undergone the "Roughness" and "General Curvature" derivations via the utilisation of ArcGIS software. The most prominent by-product derived from the momareto raster corresponds with the "Slope" derivation.

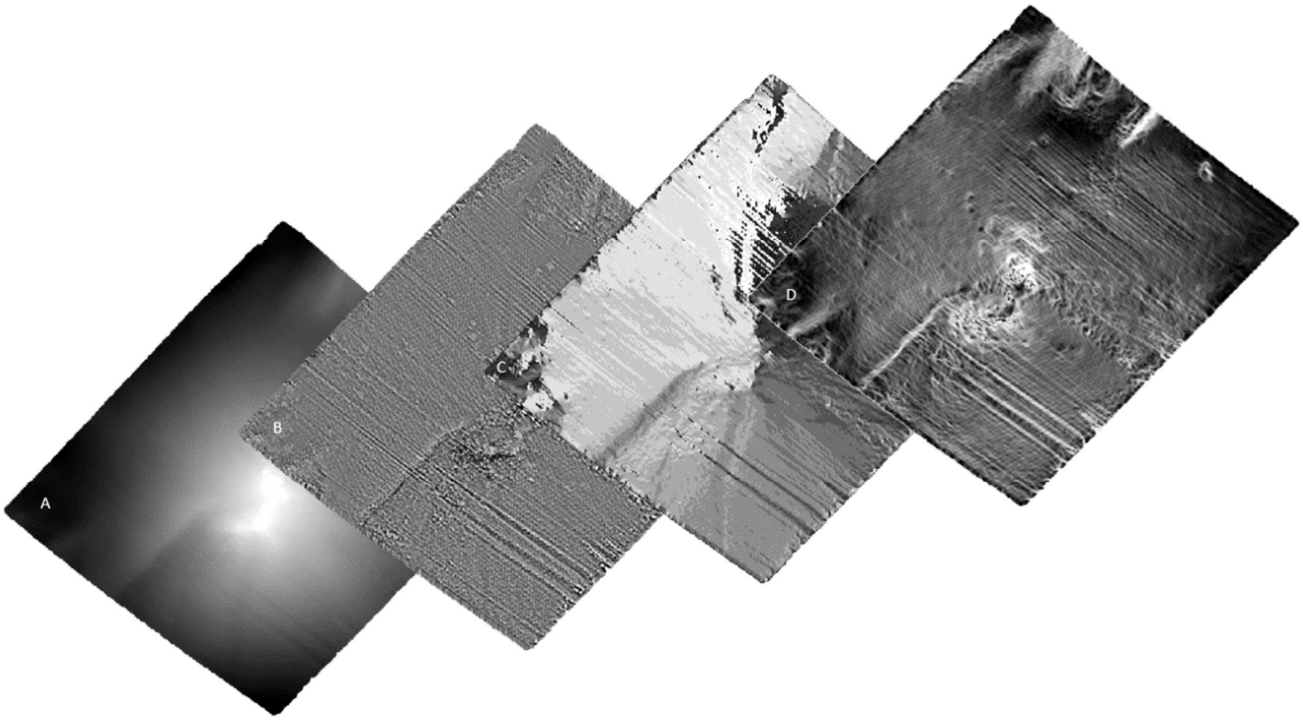

Figure 19. Example of raster derivation. (A) Camel's RAW bathymetry derived into: (B) Curvature, (C) Aspect and (D) Slope

The considerable disparities in resolution between the photomosaic and bathymetry of Lucky Strike present a challenge in their comparison and the identification of small volcanic characteristics, such as hydrothermal vents and scattered boulders. The application of Slope, Roughness, and General Curvature in this particular context serves to expose inclined surfaces, which are considered to be less suited to being the site of standing chimneys due to their unstable topography.

To execute the CNN on the raster datasets is needed to have a common way of files types stored (Robson et al., 2020). The conversion of all imagery into 32-bit floating rasters with normalised pixel values between 0 and 1 was necessary through the usage of ArcGIS.

With regard to the mosaics, due to the large surface coverage of the Lucky Strike's survey, the resulting ROV image have sizable data voids with variable NoData values. These data values could cause problems in the CNN training. As such all NoData values were reclassified to a universal value of zero.

To conclude, the original Loki Castle's mosaics presented three coloured exact images, with no distinction between each other. Therefore, only one of these was converted into a single-band grayscale image. Then the algorithm process one band per mosaic to be analysed, 32-bit float, in the greyscale, and with pixel values between 0 and 1.

Henceforth, the interpretation will be established in the form of a ruleset by the eCognition software. Every step is implemented in a single ruleset that could be run as one process. Although the goal was to make a classification procedure that was equally applicable on both datasets due to differences in data type, resolution, and coverage between the study areas, slight modifications were required, as shown in the general flowchart (Fig. 19). The following algorithms are the ones used for the interpretation of the previously mentioned processed data.

5.1.2. Segmentation

During the segmentation process, recognisable image objects are created from the mosaic. This step groups the pixels that share similar spectral context. Based on numerous configurable parameters of colour and shape homogeneity and heterogeneity.

There exist various procedures for performing segmentation, however, the *multiresolution segmentation* process is considered most suitable for the purposes of this thesis. This process is a bottom-up region-merging approach, it begins with a single pixel object and merges smaller image objects into bigger ones in succeeding segmentation steps, therefore establishing a semantic hierarchy to discover the objects of interest (Gupta & Bhadauria, 2014; Nussbaum et

al., 2008). After, the objects will be selected manually to serve as training data for the CNN to work with.

Within the multiresolution segmentation algorithm, in order to find the most suitable segmentation parameters, a trial-and-error method has been applied. Trying out different parameters before getting the right ones. These help the samples that are consequently created to share as much similarities as possible with the targeted volcanic features. The parameters utilised in the multiresolution segmentation process can be defined in a next manner (Geospatial, 2023):

- The *scale parameter*'s value determines the standard dimension of the object. This parameter affects the maximum permitted object heterogeneity. The larger the scale parameter the larger the objects are. In general, most of the mosaics studied in this thesis present a reasonable segmentation.

- The *Shape* element holds significant influence over the interaction between shape and colour criteria. By adjusting the Shape criterion, the colour criteria can be defined as the complementary value of the Shape criterion (colour = 1 – shape). When comparing the shape homogeneity criterion, the greater the shape value, the lower the influence of colour on the segmentation process.

- The *compactness* criterion is applied in cases where distinct image objects exhibit a compact nature, yet are distinguished from non-compact objects by a spectral contrast that is comparably weak. The higher the value, the more compact image objects may be.

Apart from scale, shape, and compactness parameters, the resulting segmentation is also affected by the weight of its input layers. By weighting datasets, it is guaranteed that the segmentation is not monopolised by only one dataset (Robson et al., 2015).
All these algorithms are based on individual assumptions described in table 2. Meaning that there are multiple ways to achieve similar results.

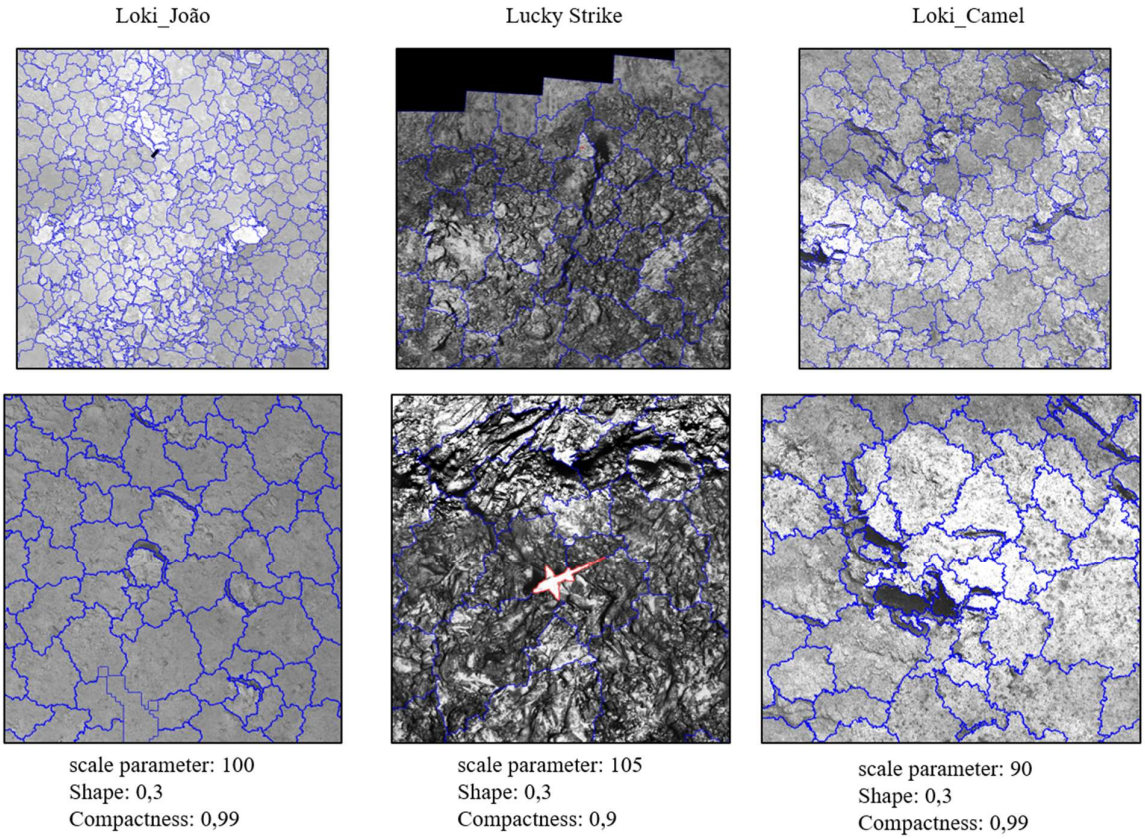

Figure 20. Segmentation parameters for each dataset. The examples reflect how the software performs different segmentations based on the context of each image. In the case of João and Camel, the scale parameter is able to adjust to smaller sizes to segment shadows, thanks to large differences on brightness values. Similarly to the level of detail of the Lucky Strike segmentation, which manages to define silhouettes as the Chimaera Monstrosa. Animal closely displayed in Fig. 1. Above it, there is an optimal capture of a chimney.

After the segmentation, a new layer is produced, where the new image-objects that it contains, are collections of pixels with common values. The domain where the ruleset classification algorithms are applied is the image-object level.

5.1.3. Convolutional Neural Networks

Also known as CNNs, the Convolutional Neural Networks are a form of ML that are increasingly used to analyze imagery of all kinds, including the ones used here, the underwater photomosaics and bathymetry.

In a nutshell (Fig. 21), its fundamental structure is made up of an input layer (the pre-processed imagery), and output layer (the heatmaps), and multiple hidden layers in between.

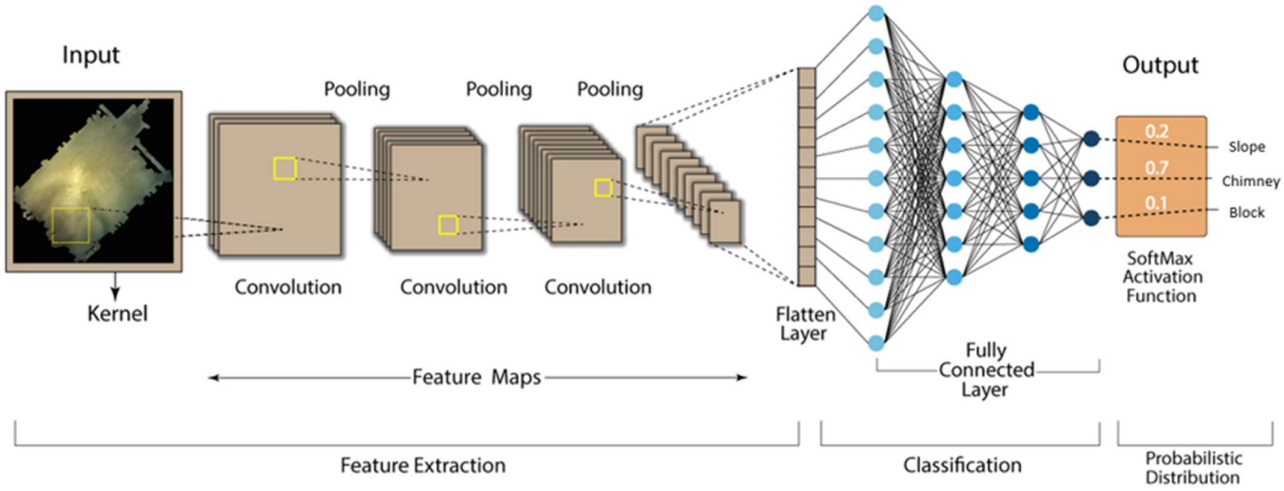

Figure 21. Basics CNN flowchart diagram. Modified from: (https://developersbreach.com, accessed on 23 May 2023).

Mathematically, a convolution is a grouping function. In CNNs, convolution happens when two matrices (rectangular arrays of numbers arranged in columns and rows) are merged to form a third matrix. The way it works in here is by extracting features from the input image using a number of convolutional layers, and then classifying the image by running the feature map produced by those first layers through one or more fully connected layers (Robson et al., 2020). These convolutional layers would work as a set of filters or kernels to the input images to extract specific features, such as textures and edges. Resulting in an attempt to mimic the way a human would evaluate the imagery.

The overall analysis can be defined as CNN Training and Classification (Timilsina et al., 2019). And it is represented in the following diagram:

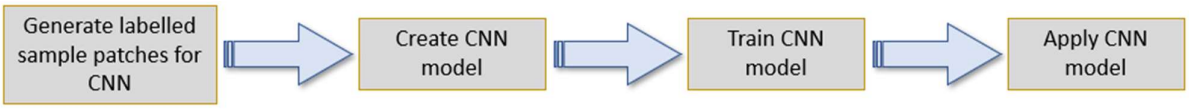

Figure 22. Workflow chart in eCognition software

5.1.3.1. Generate Sample labelled patches for the CNN model:

Upon segmenting the underwater images in eCognition, it is needed to transform the resulting segments into image objects. The image objects denote discrete areas within the image that are suitable to classification by the CNN.

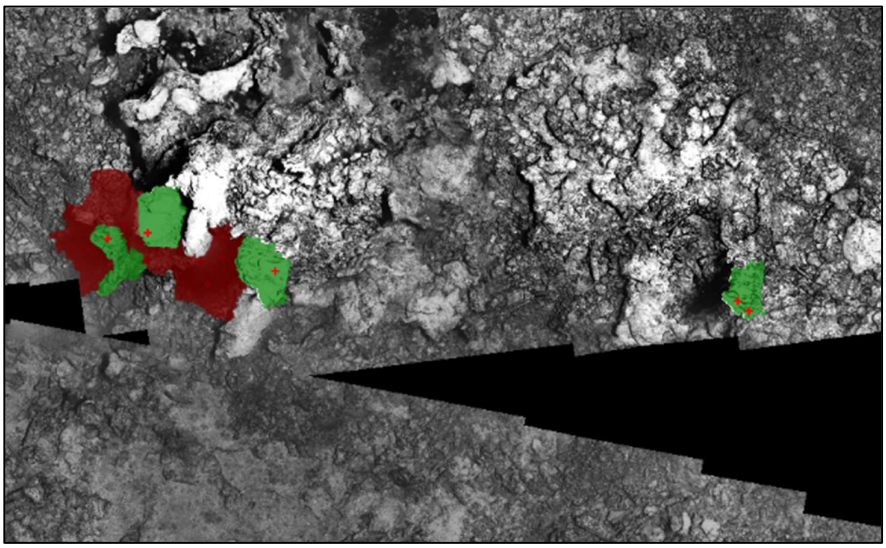

Figure 23. Example of sample labelled patches showing non-exact features boundaries while recycling the random points from ArcGIS to eCognition. Green samples refer to Chimneys and dark red samples to Shadows.

The parameters utilised for each of the input datasets are explained in the section 5.2

5.1.3.2. Create CNN model

In the first place, regarding the hidden layers, the convolution layers are the responsible for detecting patterns within the image. Each of them are composed of a collection of filters or kernels that move over the segmented mosaic performing a element-wise multiplication with the image pixels. The output of this multiplication is then added together to generate a single value that indicates the activation of a specific feature or pattern in the image (LeCun et al., 2015; Sonogashira et al., 2020). This process is repeated for each kernel in the layer, generating a collection of feature maps that capture various features of the input image.

Convolution layers are followed by pooling layers since their output is frequently too big to be processed effectively. By combining close pixels or features, these layers shrink the size of the feature maps. This improves the efficiency of the process by lowering the number of its parameters in the process. Each of these layers is made up of a collection of filters or kernels that move over the input image and conduct element-wise multiplication with the image pixels. The result of this multiplication is then added together to generate a single value that indicates the activation of a certain feature or pattern in the image (LeCun et al., 2015). There are max and average pooling layers. Max pooling picks the maximum value in a window, while average pooling computes the average. Pooling layers reduce overfitting and accelerate layer computation by reducing feature map size. In the case of this thesis, it is considered unnecessary to utilise the previously mentioned pooling layers due to the acceptable size of the feature maps and because that would reduce the feature map's resolution. Alternatively, shorter subsets were generated to get around the issue of excessive computational time required for larger images.

Fully connected layers are similar to the rest of the layers in a traditional neural network. They take the output of the previous layers and combine it to produce the final output of the network. Fully connected layers are typically used at the end of the CNN, where they map the high-level features extracted by the convolutional layers to the class labels or predictions. As a result, a heatmap is obtained, a prediction raster, which pixels vary from 0 to 1. Where higher values indicate that a given pixel is more likely to correspond to the targeted class. (Keohane & White, 2022; Robson et al., 2020; Ye, 2022).

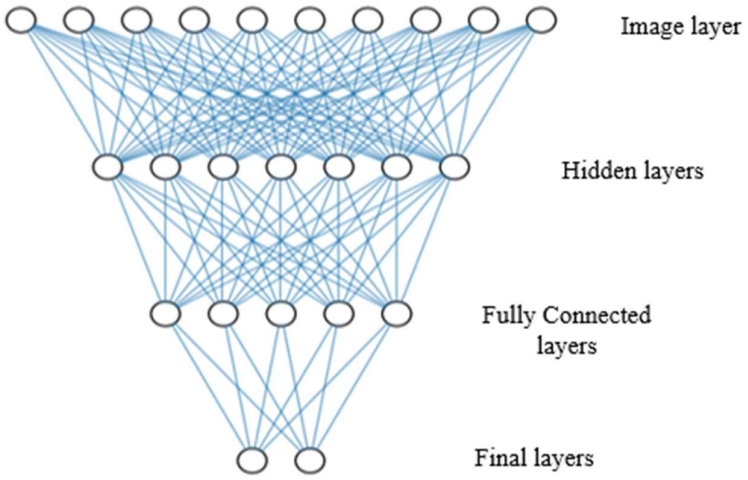

Figure 24. CNN layer architecture

In summary (Fig. 23), convolutional layers detect features or patterns within an image, pooling layers reduce the spatial size of the feature maps, and fully connected layers combine the features to form the final output of the network.

Moreover, various parameters require consideration when constructing the CNN:

- The sample patch size parameter specifies the dimensions of the rectangular sample patches in terms of pixels. The dimensions of the size parameter must correspond to the dimensions of the sample size, and the value is automatically inserted by the eCognition software based on the previously defined value to generate the sample labelled patches.

- Number of input layers.

- The output model classes, which are utilised by the model, serve as the applied classes.

- The number of hidden layers will perform convolution on the preceding layer utilising distinct kernels, resulting in the creation of diverse feature maps. Adjustments can be made within them:

- The kernel size parameter specifies the dimensions of the convolution kernel, determining its length and width.

- Number of feature maps determines the quantity of feature maps produced within the hidden layer.

5.1.3.3.Train CNN model

Training involves many separate training steps. During each iteration, a batch of samples is randomly selected and included into the model. The gradients for each weight are then computed using backpropagation, which is the calculation of a neuron's influence on a neuron in the next layer and the subsequent adjustment of its influence is performed. To conclude, the weights are optimised using a statistical gradient descent approach.

In eCognition, the training of the CNN model can be performed using the "train convolutional neural network" algorithm, where it can be imported the labelled sample patches generated in the previous step and define the following training settings:

- A *Sample folder* generation, that contains the labelled samples for the training. It is anticipated that the sample images will be 32-bit floating images within the range of (0,1).
- The *Leaning rate* parameter specifies how much weights are altered in each iteration of the statistical gradient descent algorithm. The higher the value of the learning rate, the faster the training, but the optimal minimum may not be obtained. Smaller values will slow down training processing and may cause it to become trapped in a local minimum, resulting in weights that are not even close to ideal (Timilsina et al., 2019). Default value 0.0006.
- The *Train steps* indicates the number of times this process will be implemented.
- The *Batch size* refers to the quantity of samples utilised in each training step.

5.1.3.4.Apply CNN model

Once the trained CNN model is applied to the input datasets. The resulting output may manifest as either class predictions or probability scores for each pixel that has been accurately classified as belonging to a specific class. In this case, a heatmap is generated highlighting the desired features. This map displays the features' likelihood with colours that vary from red, showing the highest probability values, to blue, indicating the lowest chance for detecting the proper features (being 0 the lowest and 1 the highest).

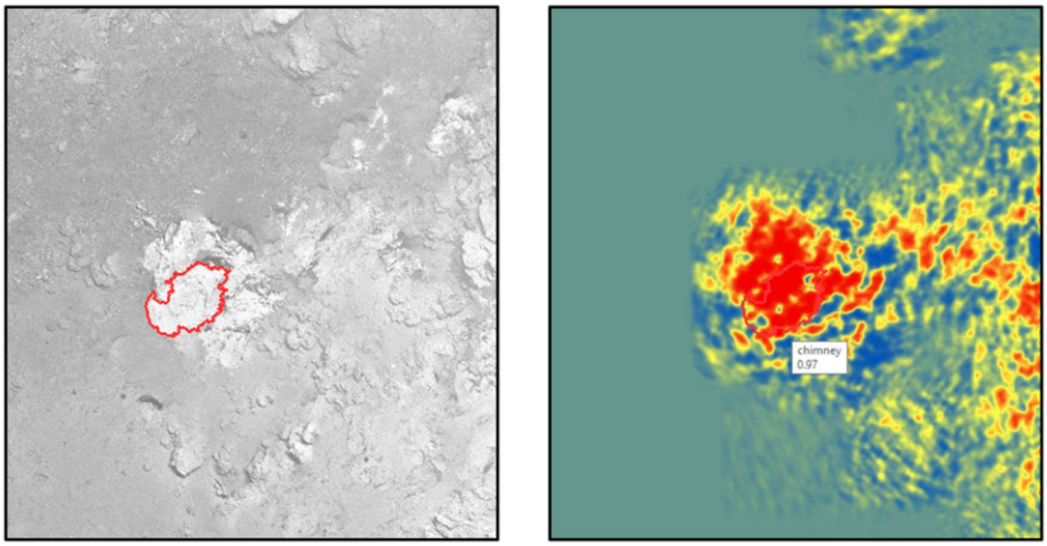

Figure 25. Chimney heatmap representation and its output value.

The parameters used in this algorithm are (Geospatial, 2023):

- The *TensorFlow model format,* which can be chosen between the eCognition model, a TensorFlow model created with eCognition or the TensorFlow (SavedModel) which is the Google TensorFlow. The parameter TensorFlow compiles various methods and models to create deep neural networks for image recognition/classification. TensorFlow uses a "graph" of processing nodes, each of which represents a mathematical operation.

- The system generates two distinct forms of *output*, which are a heatmap and a segmentation of each pre-trained class, or alternatively, those selected individually.

- As an *input*, instead of using the image layer arrays, the main image layer serves as a unique input. Being the mosaic the common main image layer for the three locations.

- The configuration for *Normalisation* determines whether the normalisation of image layers is necessary and specifies the data range for the chosen image layers. By default, the normalisation of image layers will be within the range of [0,1] and the data type will be 32-bit float. An alternative normalisation has been chosen for this study, ranging between [0 , 255].

A temporary layer is generated that serves the purpose of facilitating visualisation. The heatmap goes through a *smoothing process* through the application of a 7 x 7 Gaussian filter, which is produced by a pixel filter consisting of 7 x 7 pixels.

In conclusion, as it is important to preserve the deep learning process. The algorithm known as "Save Convolutional Neural Network" generates two distinct file types.

- The Meta Graph file is a repository storing the network architecture of a model.

- The Index file functions as a repository for the weight configurations of the model.

5.1.4. Object-Based Image Analysis

To create the proper hydrothermal feature outlines, the OBIA method makes use of the segmentation process. A bottom-up, multilevel technique that utilises statistical grouping and where the software initiates its operation by selecting a seed pixel and subsequently incorporates adjacent pixels into the growing object, provided that the object's internal consistency contrasts with the external heterogeneity. The software additionally sticks to a predefined set of shape and compactness parameters, that are previously defined, to generate larger and comparable image-objects (Blaschke et al., 2014).

One of the benefits of utilising OBIA is that the outcomes of object-based analysis tend to be more straightforward to interpret. This could be attributed to the fact that OBIA imitates human perception. An additional benefit is that the averaged representation of object characteristics during segmentation reduces the likelihood of an incorrect classification.

The resultant image-objects are ultimately classified using a mix of the deep learning heatmaps produced, the observed morphology, and the classification algorithm. Image-objects are real-world identities made of similar-valued pixels (Blaschke et al., 2014). Low-level features of image-objects can be collected to assign membership to the desired classes. Both the parameters and the thresholds for the image segmentation processes were determined manually based on personal considerations. (Robson et al., 2020). The resulting image-objects are stored in their own image-object level, which is above the pixel-level. This level is the domain where the ruleset classification algorithms are applied.

When faced with multiple thresholds and their respective algorithms, it can become difficult to determine which specific one to adjust. An alternative approach to defining the thresholds if the classes become more intricate consist in assign several conditions directly to each class. This is done from the adjusting the Membership functions (Fig. 26) in the Class Hierarchy, choosing between the following parameters for each class analysed:

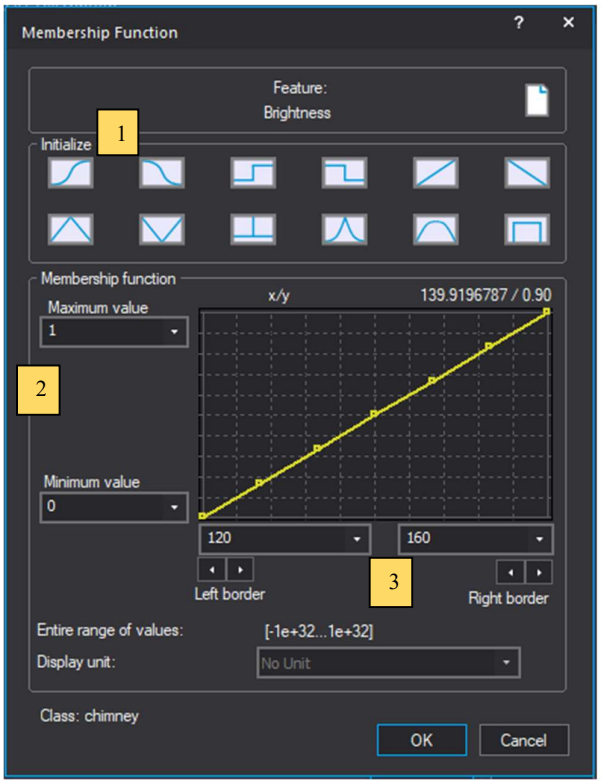

Figure 26. Parameters used to adjust each class thresholds.

- The *membership graph* (1) indicates the relation between data values and "acceptability" at that value. Utilising linear functions to specify a value in which the item definitely belongs to the class and a value in which it may still belong to a class.
- Layer *weightings* (2) reflect membership function importance. Changing the Maximum value to 0.5 gives it a 50% weighting.
- The *acceptable values* (3) refer to the maximum and minimum values that are taken into account during the analysis.

Tweaking these parameters results in an object that closely matches the appearance of a feature that has been manually defined. The previously mentioned entities are extracted through the utilisation of an algorithm, specifically the "export vector layer" algorithm, which exports the shapes of the entities in the form of polygons, thereby generating a shapefile (*.shp).

To achieve the desired comparison between the manually delineated polygons that define the hydrothermal features and the objects generated from eCognition. The shapefiles undergo final processing in ArcGIS, where a concluding procedure will be executed.

5.1.5. Classification Accuracy Assessment

The final accuracy is an outcome of the combination of the two stated techniques for image classification, (OBIA and CNN). The Accuracy Assessment of the classification relies on the confusion matrix generated from two distinct sources, namely the "ground truth" data, manually generated, and the eCognition outcome (OBIA_raster), which are the classified rasters (Robson et al., 2020; Timilsina et al., 2019). The absence of reliable and verifiable ground-truth data poses a challenge in evaluating the accuracy of manully mapping outlines. This study draws upon the comprehensive knowledge and expertise gained from the description of hydrothermal vent features, as detailed in sections 2.2.1.1 and 2.2.1.2 . The study aims to develop distinct outlines with a reasonable degree of certainty and assurance, displaying on a confusion matrix, which is a table layout that allows visualization of the performance of the algorithm

In order to execute this combination, a set of random points is generated within arcGIS and designated as either "chimney" or "non-chimney" features, alongside other hydrothermal features. These designations were based on the manual mapping outlines produced within the scope of this thesis . Subsequently, a comparison was made between the aforementioned points and the results obtained from OBIA_raster. This comparison led to the determination of the following error terms in the confusion matrix (Robson et al., 2016):

- User's accuracy: This error of commission shows the percentage of the final classification that was a chimney.
- Producer's accuracy: This error of omission describes the percentage of actual chimney area that was successfully classified.
- Overall accuracy: This takes into account the accuracy of both the user and the producer, and presents the proportion of correctly classified points as a percentage.
- Kappa coeficient: This evaluates the agreement between the assigned classifications and the actual ground truth pixels, this is a crucial indicator of the classification's accuracy, as it helps to rule out the possibility of the classification being a result of random chance.

The following analysis involves a comparison between the confusion matrices of manual and automated mapping. The purpose of this comparison is to determine the validity of the approach utilised in this thesis. A comprehensive discussion will be presented to address this matter.

5.2. Parameters utilised

The objective of this analysis was to employ the OBIA ruleset to categorise hydrothermal features in every study area, with the aim of evaluating the chimneys inventory creation capacity of CNN-OBIA. The aim was to create a basic ruleset that could be implemented across three different study areas characterised by diverse topographies, resolutions, and lighting conditions. Consequently, the adjustment of thresholds such as brightness, standard deviation of each image layer, and depth, which may vary across each area, was performed on an individual basis.

It is noteworthy to emphasise that the main parameter setting employed to attain a significant classification in this thesis is the one explained hereafter, in spite of the existence of alternative methodologies that may achieve comparable results.

- The segmentation process has been performed using the following settings:

Table 2. Segmentation parameters.

Dataset	Scale	Shape	Compactness	Layers	Classification
Lucky Strike	105	0,3	0,9	mosaic	Bacterial mats, chimney, smoke/ shadow, wrinkles
Loki East (João)	100	0,3	0,99	mosaic and bathymetry	Chimney, block, slope
Loki West (Camel)	90	0,3	0,99	mosaic and bathymetry	Chimney, block, slope

- Lucky Strike's segmentation produced objects that match into the intended structures, particularly in cases where these structures exhibit discernible variations in their luminosity and shapes within the image.
- Loki East and West is affected by the same principle, thus obtaining suitable segmentations even for blocks as they are scattered along the smooth surface that surrounds the vents on top of the two mounds.

As can be seen, the values shown in Table 2 show strong similarities, since all sharing same resolutions and are set in the black-and-white spectrum. In every instance, the classification of small objects becomes challenging by setting larger scale parameters. The shape criterion

has been adjusted to a relatively reduced threshold due to the increased impact of colour when working with monochromatic images. Whereas the compactness criterion is chosen to have the maximum value, as pixels vary abruptly throughout every mosaic analysed, smaller values would result in more frequent outstanding appendices.

- Labelled sample patches were produced using two different procedures:

- For the Lucky Strike's dataset, an earlier and unsuccessful approach was tried before choosing the multiresolution segmentation as the most appropriate method. It consisted of generating polygons covering the features to be processed later. These polygons had random points generated in ArcGIS. Buffer zones were established based on the identified points to delineate areas with similar characteristics that share a common space. These buffers meant that the training data expanded over the target classes but simultaneously it did it over larger parts of non-target classes, meaning the training data was blurred.
Subsequently, the random points got recycled using the Assign Class algorithm in eCognition, taking into account the mentioned random points which overlap within the segmented new features.
- For the rest of the segmented mosaics, samples were chosen manually. These samples remain related with the many classes that are designed to be examined, whether independently or with the "Brush" option. And finally, an algorithm in the ruleset converts the sample objects to classified objects.

- In order to create the CNN model, the following parameters have been used:

Table 3. CNN parameters

Dataset	Sample patch size	# input layers	# hidden layers	Kernel size	# feature maps
Lucky Strike	32	1	2	13, 14	80, 50
Loki East (João)	128	1	2	5, 5	80, 80
Loki West (Camel)	64	1	2	12, 12	80, 80

Each sample patch size was assigned after conducting multiple trials to determine the optimal size that produced the desired heatmap. The sample size was defined at the beginning of the deep learning process using the algorithm “update variable”. Finer results have been observed when using powers of 2.

- The input layer employed for the three regions is the mosaic, as it is the one that contains more information to work with.

- The mosaic is chosen as the input layer for the three regions due to its capacity to provide an increased quantity of information for processing.

- The recommended approach in this case involves the application of two hidden layers for all processes. The utilisation of different amounts of hidden layers is subject to unfavourable interpretations.

- Within them, the determination of the kernel size depends on the total number of classes that the CNN is intended to classify. This number is the result of subtracting the sum of the kernel sizes from the original sample size.

- The determination of the number of feature maps is also dependent on a trial-and-error approach.

As explained in section 5.1.3.2. For this thesis, Max pooling was not applied, as the highest resolution in the results was sought.

- The training parameters were as well chosen from an empirical methodology, obtaining suitable heatmaps by keeping the learning rate for the three datasets in its default value (0,0006). The number of iterations this process is repeated was 8000 for the Lucky Strike mosaic and 4000 for both Loki’s datasets. Respectively, the quantity of samples utilised in each training step (the Batch size), were 20 and 16.

- As the final output of this methodology has to be compared across the different datasets. The desired result type is a visualisation in the form of a heatmap. The CNN was implemented using the eCognition model for the TensorFlow format. The normalization values that define the data range of the selected image layers are [0, 255].

- OBIA

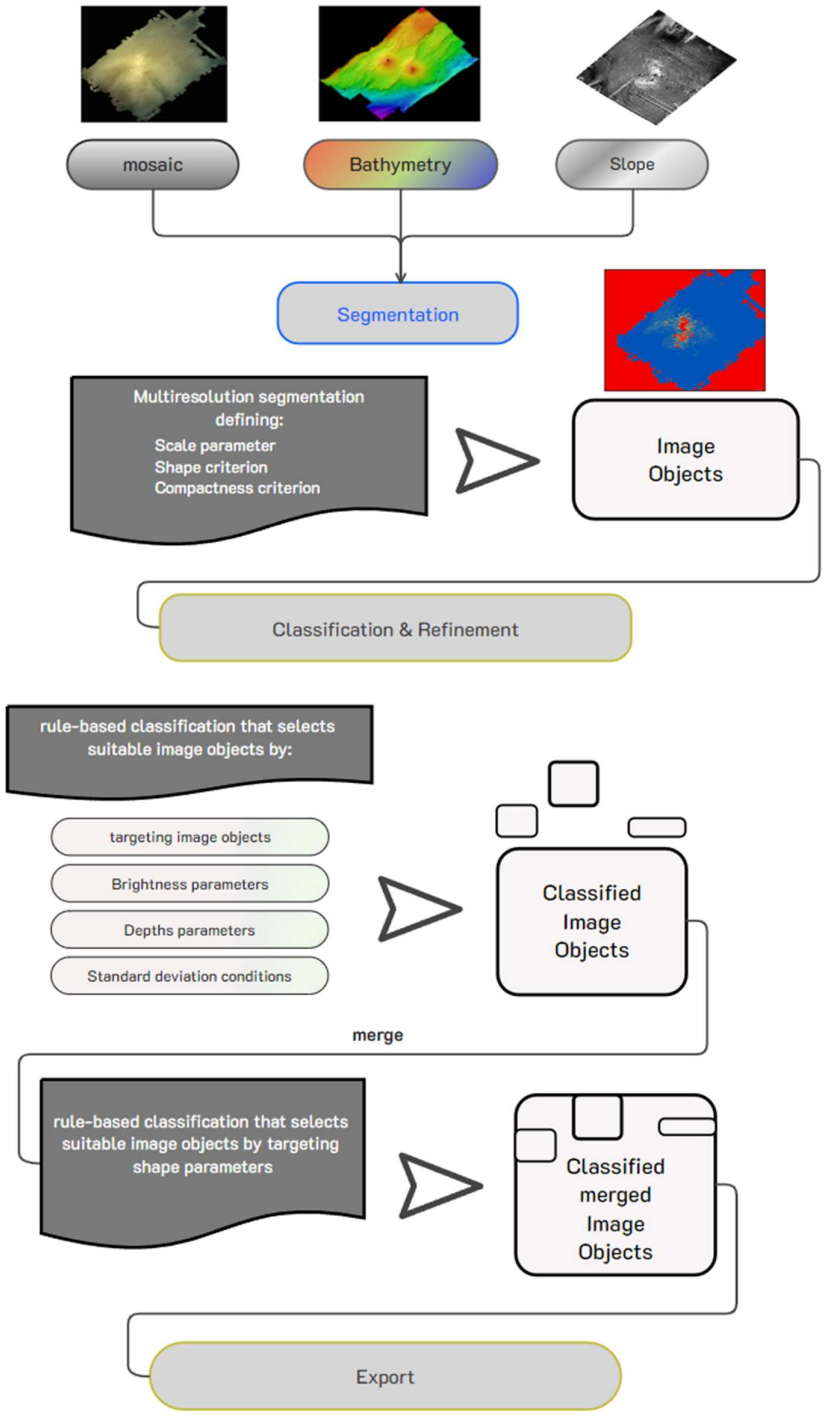

Figure 27. OBIA workflow applied for the classification.

Using the segmentation parameters that were previously discussed. The refining process that is to come involves a set of thresholds or maximum acceptable values that are determined on an individual basis for each input dataset:

Table 4. OBIA's maximum acceptable values

Dataset	Brightness	Depth (m)	Mean	Slope	Area (m^2)	others
LS bacterial mat			bac mat > 0,54 block > 0,20			
LS block	< -35		block > 0,20			
LS chimney			chimney > 0,64		< 1,01	border to shadow > - 0,01
LS smoke/shadow	< 20		smoke > 0,75	Slope*		
LS wrinkle			wrinkle > 0,39			
LE João slope			Slope > 0,21	< 31		
LE João chimney	> 140	> -2312	chimney > 0,9			
LW Camel chimney	> -706	> -2314	chimney > 0,68			

In addition, among the admissible values, the minimum acceptable values serve as the lower limits, delineating the extent to which the conditions continue to classify the objects.

Upon achieving satisfactory classification of image objects, objects that share the same designation are grouped together through the implementation of the "merge region" rule. This rule is responsible for the gathering of all image objects within the image object domain. The final step of the classification procedure requires the extraction of the shapes of the image objects and their exportation into a vector file. The algorithm "export vector layer" is utilised to create the previously mentioned output. Thus, a new raster that includes the recently merged polygons is generated, and subsequently stored in a distinct pathway in the format of a shapefile (*shp).

- Accuracy Assessment

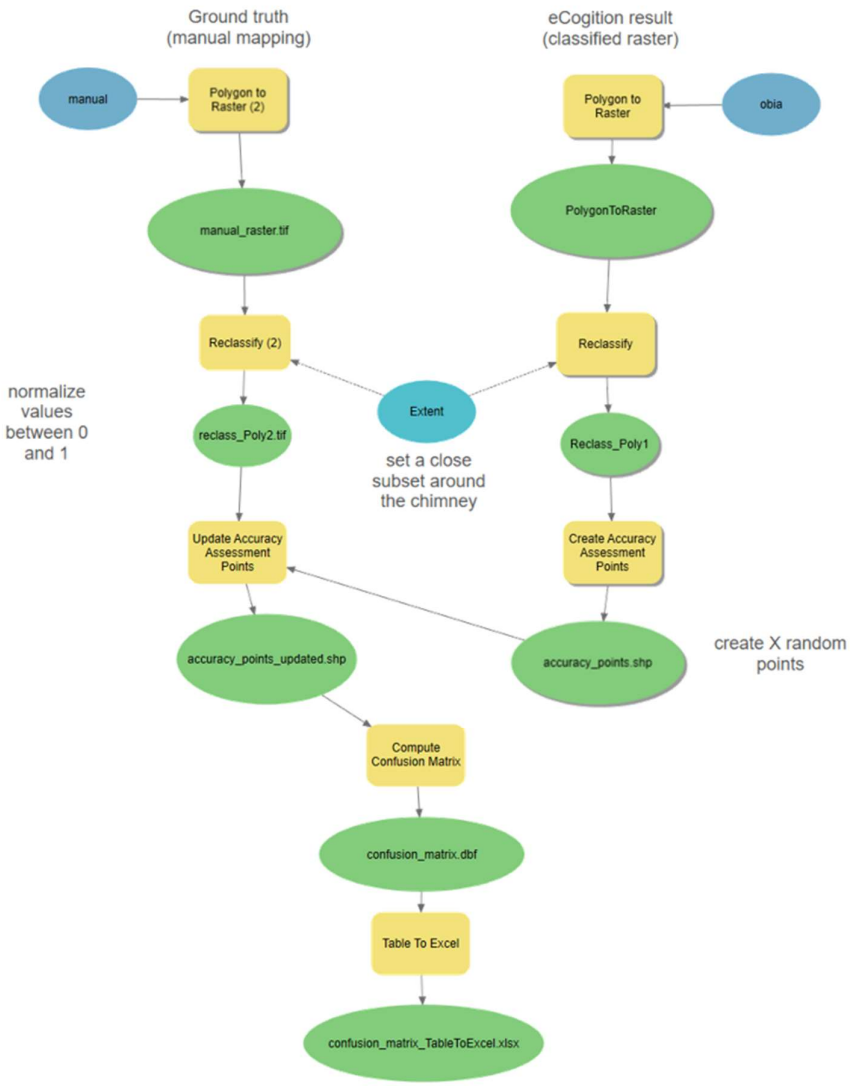

Figure 28. Confusion Matrix model applied for the assessment of accuracy.

The shapefile produced by eCognition software are imported in ArcGIS. In order to perform a Confusion Matrix Computation, the outlined workflow has been followed (Fig. 28). Generating 9000 random points, they have been assigned to either “chimney” or “not-chimney” features using the manually created outlines. These outlines inevitably are very

The random points were then compared with the OBIA_raster outputs, with the objective of determining the errors, which constitute the desired results.

6. Results

Initially, it is essential to highlight that the efficacy of the CNN process in accurately classifying data has a direct impact on the interpretation of identified features and consequently influences the level of satisfaction with the generated heatmaps.
The heatmaps that are presented below have been considered as the most suitable for accurately classifying chimneys.

The process of resolving this task was the most time-intensive aspect of the thesis project, requiring significant condition adjustments to various parameters, and algorithm trial-and-error approaches in order to ultimately generate the foundational heatmaps necessary for analysis.

As shown in the Figure 29, the heatmaps have effectively identified the most significant features for the purpose of this study.

The primary objective of this thesis was to evaluate the feasibility of formulating a methodology, rather than achieving exceptional outcomes. As such, the result that was reached is fairly straightforward.

The heatmaps chosen for evaluation of their efficacy are those that optimally delineate the boundaries of the objects being identified, based on the parameters incorporated in order to create the CNN (Table 3).

Table 5. Accuracy Assessment final values.

Dataset	User's Acc.	Producer's Acc.	Kappa Coefficient	Overall Acc.
Lucky Strike	0,29	0,36	0,39	0,51
Loki East (João)	0,64	0,7	0,67	0,99
Loki West (Camel)	0,73	0,76	0,75	0,99

Three rasters, labelled as OBIA_rasters, were generated from the heatmaps and incorporated into the ArcGIS model (Fig. 28). The resultant values were calculated utilising the confusion matrix, as elucidated in the Methodology section. The evaluation of the confusion matrix is centred on the validation polygons (OBIA_rasters) rather than the training polygons (manual).

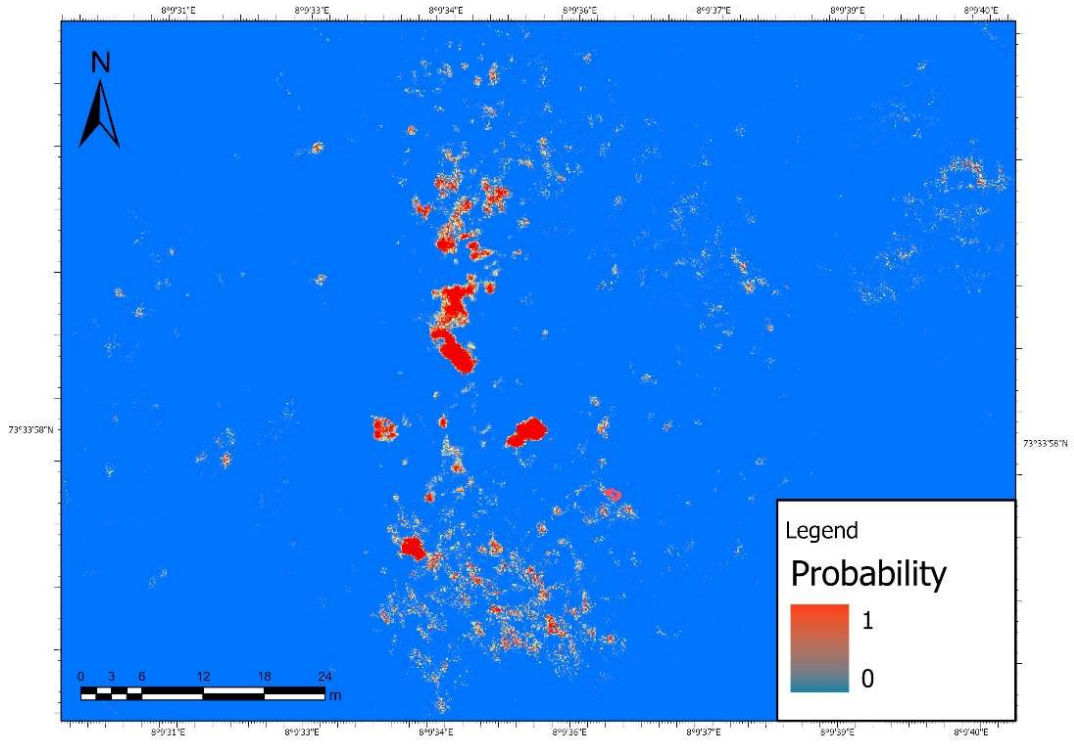
N
Legend
Probability
1
0
0 3 6 12 18 24
m

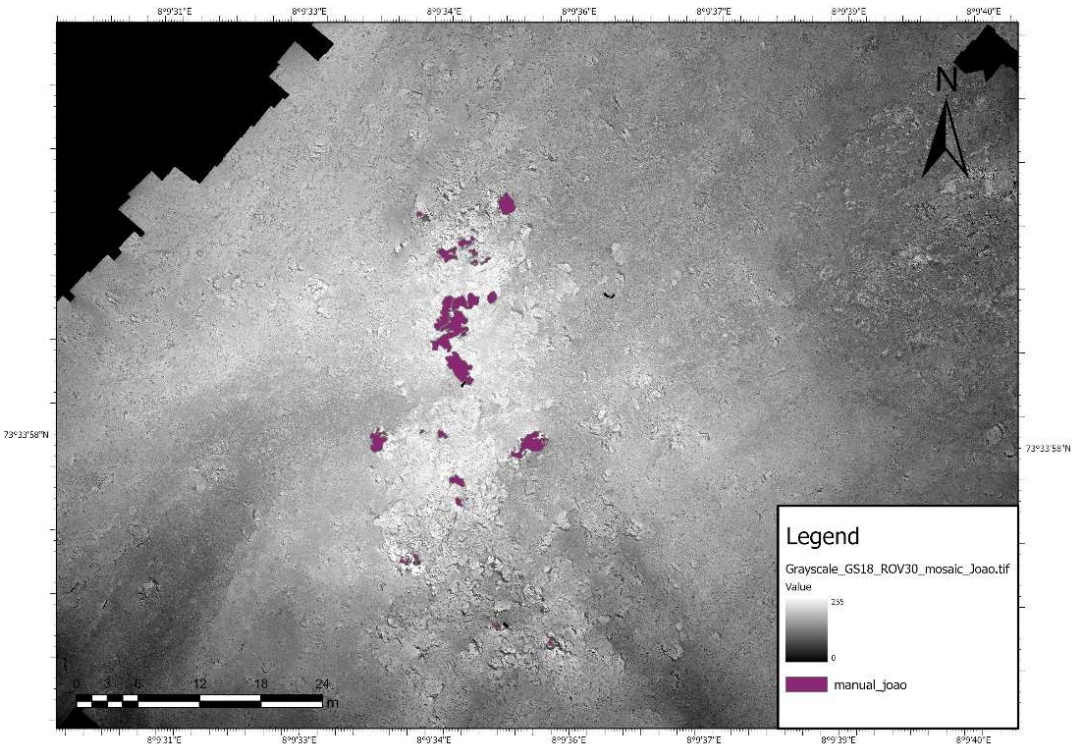
N
Legend
Grayscale_GS18_ROV30_mosaic_Joao.tif
Value
255
0
manual_joao
0 3 6 12 18 24
m

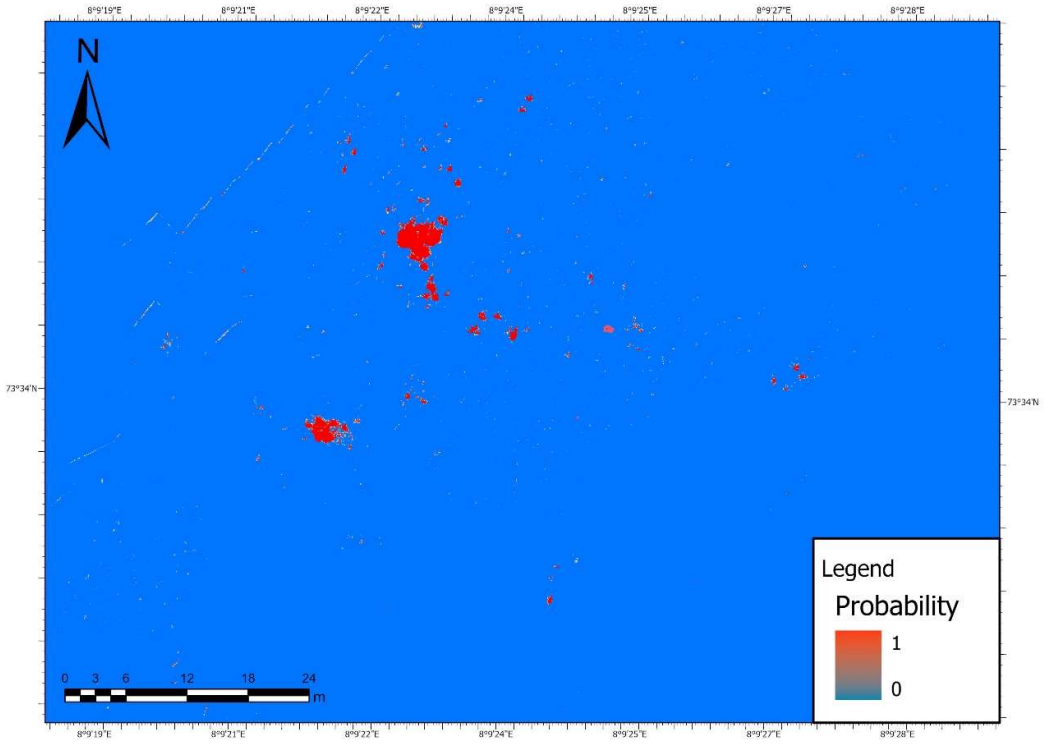
8°9'19"E
8°9'21"E
8°9'22"E
8°9'24"E
8°9'25"E
8°9'27"E
8°9'28"E
N
73°34'N
0 3 6 12 18 24
m
Legend
Probability
1
0

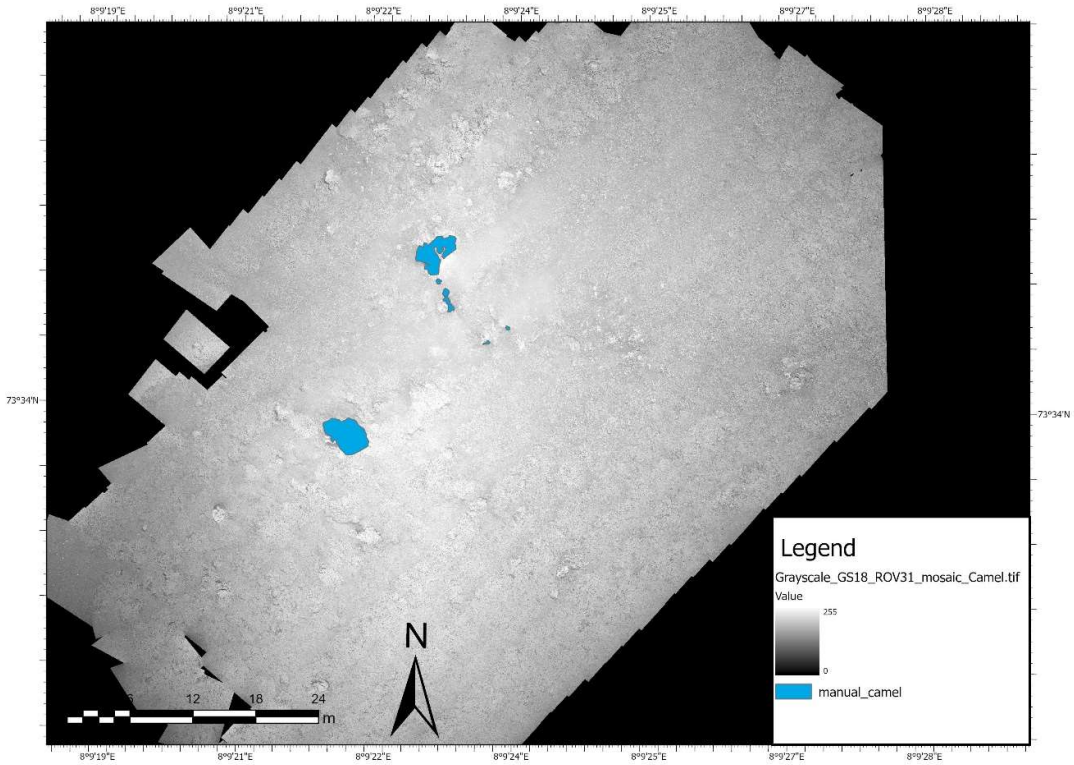
8°9'19"E
8°9'21"E
8°9'22"E
8°9'24"E
8°9'25"E
8°9'27"E
8°9'28"E
73°34'N
N
12 18 24
m
Legend
Grayscale_GS18_ROV31_mosaic_Camel.tif
Value
255
0
manual_camel

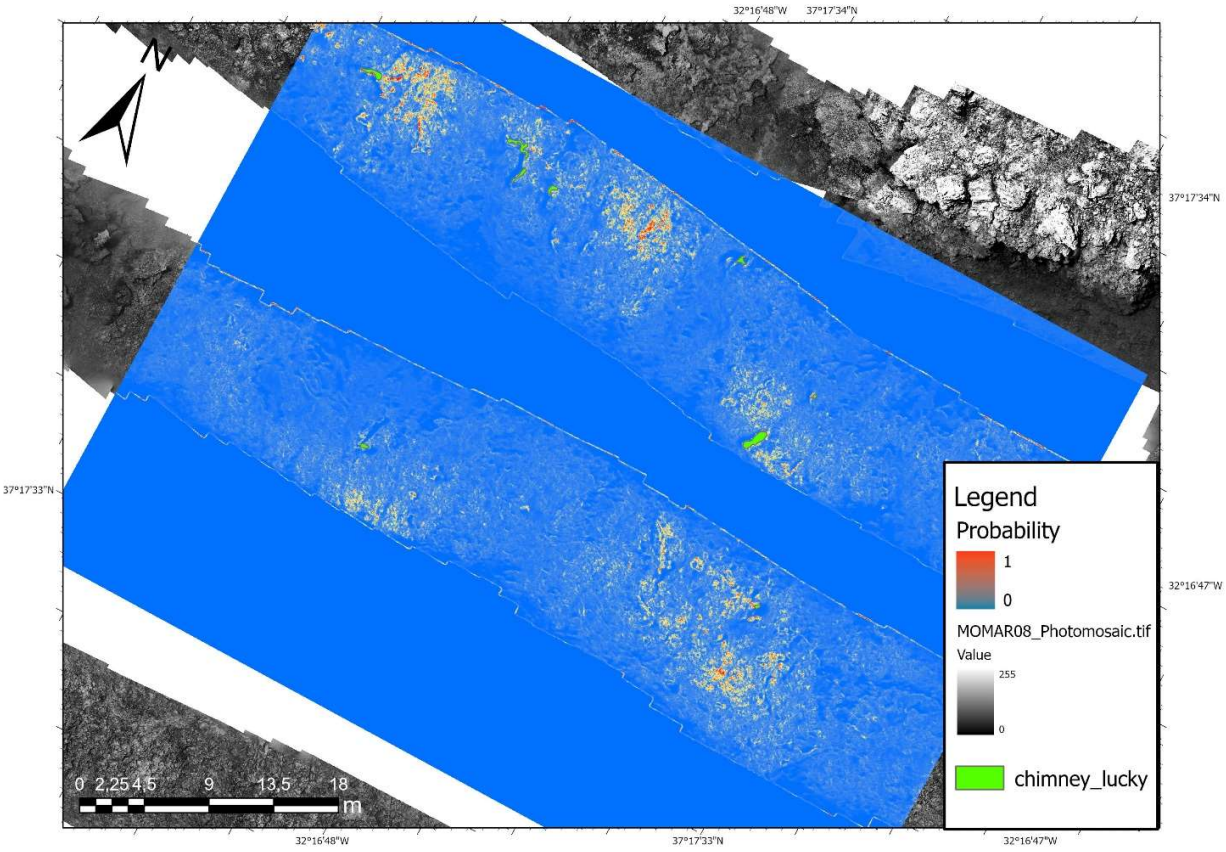

Figure 29. Final chimney heatmaps of the three study regions and the manual outlines produced as reference.

These values are discussed in the forthcoming section.

7. Discussion

The present chapter is divided into two distinct sections. The initial section focuses on the utilisation of the CNN-OBIA methodology and deliberates on the choices made during the process of segmentation and classification. Regarding this matter, the challenges posed by various types of training data are discussed, as well as the limitations of this study and possibilities for improvement. The remaining part of the classification-focused discussion looks into the accuracy of the ruleset-based classification.

The second section of the discussion centres on the ethical and environmental implications that arise when achieving a more precise cartography of the ocean floor. In conjunction with a comprehensive understanding of the actual knowledge gaps that exist as well as of the current legal setting and a description of the imminent future in the deep-sea mining sector.

7.1. Technical Discussion

In this thesis, it has been explored the potential of machine learning methods as instruments for the management of deep-sea resources. Although this thesis is one of the first of its kind, the results obtained indicate promising developments and highlight the influence of artificial intelligence in this domain. This discussion section aims to provide a broader perspective on the significance of these findings, the limitations of the study, and the potential future directions for research in this field.

The findings presented in this thesis indicate that ML techniques, particularly those employed with the three mosaics, are effective in the classification of deep-sea features. The efficacy of these methods has been demonstrated and has surpassed expectations, providing new perspectives on the research and facing exploitation of these unfamiliar ecosystems. Through the utilisation of ML algorithms, a detailed examination using of relative extensive datasets has been achieved, taking into consideration environmental parameters, distribution patterns of landforms, and characteristics of habitats, resulting in an improved understanding of the deep-sea.

7.1.1. Classification and evaluation of deep-sea hydrothermal features through CNNs and OBIA integration

The practical knowledge acquired through the handling of underwater imagery led to determine that the utilisation of object classification represents an improved methodology for the interpretation of hydrothermal characteristics, in contrast to the combination of diverse satellite bands like satellite remote sensing has traditionally done.

The present study has developed a CNN-OBIA classification approach that shows a notable level of accuracy in two of the three separate study regions.

Being the main objects sought since the beginning, the chimneys are also among those with the most discernible characteristics of all the objects that have been assumed as possible targets from the very start. These characteristics, which are listed in Table 4, mostly respond to differences in the image, which in the end is the main data source for the study. The differences include the compactness of its morphology and the abrupt fluctuations in luminosity caused by the artificial lighting. The chimneys exhibit a range of luminosity, ranging from bright white illumination at their uppermost portions to significantly darker shades, located just next to them (Fig. 20 and Fig. 23). Thus, the heatmaps depicting the interpretation of the chimney, which was the one predominantly utilised in this study, have attained a considerable degree of precision. Demonstrating well-defined boundaries that enable comparison with manually interpreted counterparts, as part of a subsequent Accuracy Assessment.

Nonetheless, alternative heatmaps have been generated, though not employed in the final evaluation. Hydrothermal features, such as bacterial mats, could be identified by analysing brightness values of 100 ranging from 0 to 255 and selecting smooth surfaces during the CNN procedure.

However, the heatmaps generated by these features exhibited a significant quantity of bacterial maps that were determined to be unreliable. The reason behind the decision to ultimately stay away from employing it.

Analogous methodologies have been applied to hydrothermal characteristics, including dispersed blocks, wrinkles resulting from vulcanism, and general slopes that can be distinguished based on coarse variations in luminosity.

The CNN-OBIA method generated maximum accuracy scores of 76 % for chimney features in one study region (Camel). This suggests that the integration of deep learning and OBIA is a reliable and precise approach for defining the boundaries of venting activity in complex hydrothermal settings.

The João hydrothermal setting can be considered as a comparable scenario.

However, in the context of the Lucky Strike mosaic interpretation, the kappa coefficient obtained along with were comparatively lower than that of the other two datasets. Meaning that the agreement between assigned classification and actual ground control points is poorly evaluated. This occurrence can be explained by the comparatively greater dimensions of the previously mentioned input, in addition to the existence of a greater number of intricate features spanning the majority of the mosaic. In contrast to the smoothed and almost unaltered surfaces observed in the Joao and Camel hydrothermal mounds. (Zoom-in Figure 17 to compare mosaic surfaces.)

7.1.2. The datasets utilised for training and limitations of this study.

Despite having worked with this limited source of training data, a significant progress has been made. However, further enhancements can be made by incorporating additional information to augment the existing dataset.

This study used high-resolution underwater mosaic to train the CNN models to extract patterns and develop predictive feature mapping models. Moreover ML also requires bathymetry data, which describes the seafloor's depth and topography. Bathymetry data helps map the distribution and interconnectedness of deep-sea ecosystems. Predictive models based on bathymetry data can help predict deep-sea feature occurrence and spatial extent. By combining the seafloor's three-dimensional properties, bathymetry and mosaic data can improve feature mapping. The only disadvantage is that high-resolution bathymetry is scarce. Therefore, it becomes a limitation to work with coarser resolutions in bathymetry. (Fig. 30)

While the results of this thesis are encouraging, it is essential to acknowledge its limitations. The investigation of the ocean floor represents a challenge in it's own. Although, ongoing advancements in research are concentrated on addressing some of the most prevalent constraints encountered during underwater research.

Firstly, the study is constrained by the availability and quality of data, as deep-sea environments remain largely unexplored. Future research efforts should focus on expanding data collection and improving data accuracy to enhance the robustness of ML models.

The resolution of images tends to decrease significantly when analysing images at such depths. For instance, the resolution of these datasets represents a significant factor in altering the outcome. The reason for this can be attributed to the analysis of a single region using datasets that vary greatly in nature, such as photomosaics and bathymetry. The figure depicted below illustrates the varying resolutions within a example region of the Lucky Strike datasets.

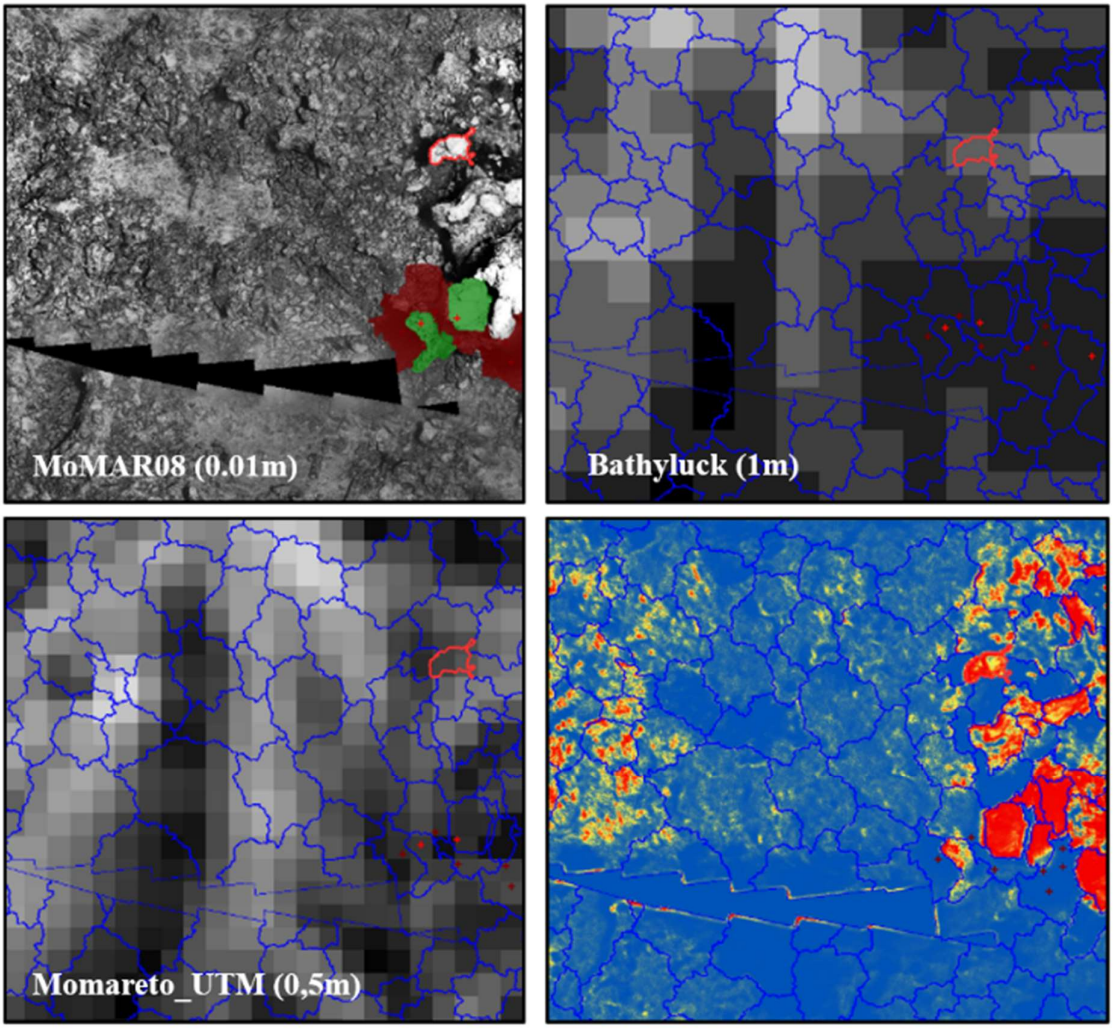

Figure 30. Comparison of different resolution from a section of Lucky Strike Hydrothermal Vent Field. Outlined in red is a segmented object that serves to compare the difference in resolution between the mosaic and the bathymetry. In the bottom-right corner there is heatmap produced out from the mosaic. The values given in metres are the resolution of each of the datasets..

7.1.3. Potential for improvement

In the future, there exist numerous potential possibilities for further research within this particular academic domain. The incorporation of more sophisticated machine learning techniques has the potential to improve the predictive capacities of models and facilitate more precise evaluations of the behaviour of deep-sea resources.

Furthermore, the incorporation of real-time data streams and the development of autonomous data collection platforms could facilitate continuous monitoring and adaptive management strategies. The Saildrone Surveyor (Gentemann et al., 2020) and the Eelume robot developed by NTNU are two examples that have been put forth to support the Seabed 2030 Project, as mentioned in the Introduction.

Throughout the process of composing the thesis, a research attempt was conducted into the feasibility of employing an alternative technique, namely ESRGAN, which tries to enhance the resolution of datasets through programming. The issue at hand pertains to the fact that the technique was originally intended for the purpose of interpolating pixels that are associated with colour images. And underwater images, especially bathymetry, are never in colour. Still, this suggests the continuing room for improvement.

7.2. Ethical Discussion

This thesis is conceived to be one more tool from academia to ensure the protection of the marine environment as a whole. It focuses on the mapping of the seabed to divulge the tremendous natural wealth that this environment contains and of which we know so little. And thus, this study aims to contribute to the current social pressure on international organizations such as the International Seabed Authority (ISA) to pause and implement regulations in this incipient mining process until environmental protection requirements have been met. This will prevent further disastrous ecological harm that the planet has experienced before. This thesis aims to serve as further evidence that research is a valuable means of ensuring the sustainable progress that is necessary.

The utilisation of AI and ML to quickly and conveniently assess imagery and related environmental data has led to a growing number of questions regarding how society will manage this inflow of novel data.

In light of recent advancements across various fields, there has been a growing interest in identifying more efficient methods for extracting valuable resources. Gaining an in-depth comprehension of deep-sea ecosystems is imperative in mitigating humanity's tendency to exhaust all available resources. Thus, it will ensure that the neceessary measures for preventing any potential adverse impacts are adequately considered, prior to it being too late to do so. Hence, given the numerous uncertainties surrounding the forthcoming underwater large-scale mining process, it is crucial to conduct more extensive scientific research before embarking on any sensitive industrial activities.

Even though models are useful tools to analyse the potential effects of deep-sea mining, to completely appreciate the nature and extent of the impacts it would be necessary to conduct and carefully monitor mining tests.

7.2.1. Knowledge gaps

In spite of certain pre-existing knowledge, such as the instances listed in the section 1.3 (Impacts of human activity on deep-sea ecosystems), there is a lack of established ecological baselines for ecosystems that will likely be impacted by deep-sea mining. In order to address this issue it is important to fully understand the temporal dynamics, thereby enabling the differentiation of mining impacts from natural variations (Clark et al., 2020).

More precisely, it is recommended that research efforts refer to every level of the water column, with a particular emphasis on the bathypelagic and abyssopelagic regions, from depths of roughly 1,000 metres to the uppermost layer of the seafloor. This is due to the potential co-occurrence of seafloor collector plumes and dewatering plumes in these regions. An additional point of uncertainty arises in the development of the study of metal leaching from ores onboard the mining vessels and the assessment of optimal techniques for monitoring the spatial and temporal impact of these processes within the discharge of dewatering fluids. The impact of this is dependent on the characteristics of different procedures used and mining scenarios. Empirical acquisition of certain significant inputs, such as physical oceanographic and sediment parameters in mining regions, is necessary for these models (Drazen et al., 2020).

To exemplify it, according to the report produce by the (Directorate, 2023), slightly over half of the study areas in Norway have been mapped using ship bathymetry as of December 1st, 2022. This offers a foundation for generating high-resolution (25 m or less) topographic maps of the ocean floor. It is important to ensure uniform resolution across the entire investigation

area. Accurate calculation of the surface area of mountainous regions that satisfy the conditions for the development of manganese crusts is key. Simultaneously, this serves as a fundamental prerequisite for AUV expeditions aimed at locating ancient sulphide deposits situated to the east and west of current spreading ridges.

With regard to these polymetallic sulphide deposits, its mining would be concentrated on inactive sectors due to functionality and safety considerations. Prior to any exploitation, it is vital to determine whether hydrothermal activity ends temporarily (dormant) or permanently (extinct), as their respective habitats encounter dramatic changes (Van Dover et al., 2020).

7.2.2. Environmental Repercussions

Building upon the impacts outlined initially in the introductory section 2.3 (Hydrothermal Vents as potential mining sites), the required additional investigation has been organised into three separate units based on each phase of the entire mining process.
Throughout this thesis, it has been emphasised how crucial it is during the *exploration stage* (Clark et al., 2020) to understand the range of natural variations in the environmental baseline parameters and differentiate human-induced changes from natural conditions in the environment.

The following paragraphs will focus on phases that have not yet begun (Guo et al., 2023): Throughout the *extraction stage* the ecological factors centre on the methods employed for mining and the resulting tailings. It is imperative to use the current monitoring techniques and uphold existing theoretical counselling in order to assess the ecological consequences of mining operations in the long-term. This approach is necessary to maintain sensitive environmental indicators within acceptable thresholds, as well as to validate the accuracy of projected impacts on the environment.
In the *closure stage*, the primary objective is to rehabilitate the mine site's ecosystem, specifically in regards to the original flora and fauna. Whilst the full repercussions of mining activities remain incompletely understood, certain factors require consideration. These include the extent of the mining activities in relation to the overall oceanic region, the effects of mining activities from epipelagic to benthypelagic flows during varying seasons, the proximity of human settlements to the mined regions and the potential effects on fishing or other commercial activities in the affected area.

7.2.3. Current state of development

The protection and management of the rare and vulnerable hydrothermal vent ecosystems is already acknowledged. As described in the section 2.3, there are multiple efforts from international bodies to ensure correct practices both along international waters and within the national EEZs (Fig. 29).

However, it is noteworthy that certain institutions have faced criticism for their attempts to hasten the initiation of deep-sea mining, despite the apparent scepticism of such ideas, highlighted by this article (McVeigh, 2023) in The Guardian.
Historically, conflicts of interest have posed a challenge in achieving objectives related to complex situations such as seabed mining. In contemporary times, there is an extensive history of diplomatic relations between nations and the potential advances in technology facilitating responsible practices in sustainable seabed mining. Considering this, achieving a mutually beneficial consensus should not prove to be an impossible task. Even so, the following is a summary of the context that shows the complex situation surrounding seabed mining.

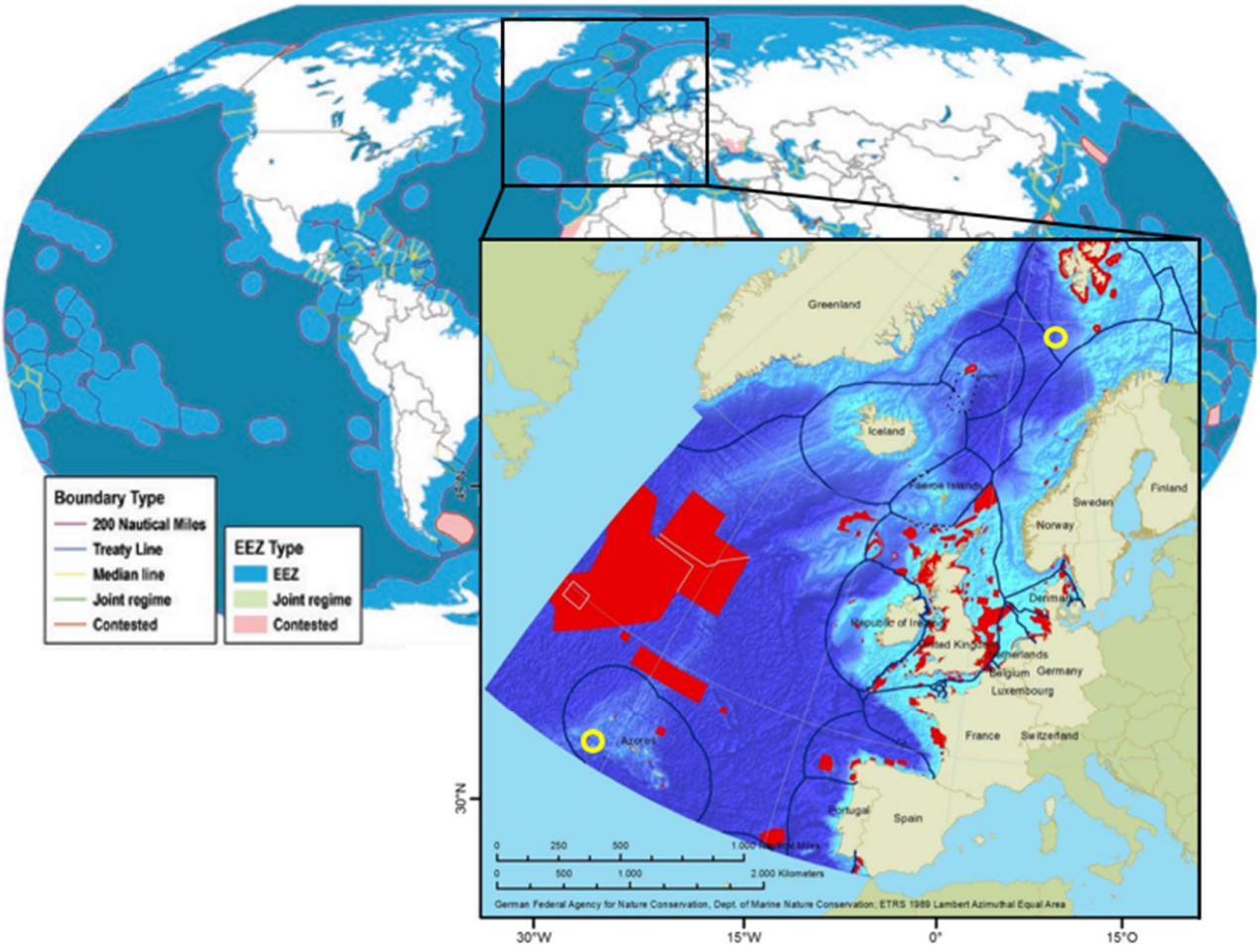

Figure 31. Maritime Boundaries Geodatabase: Maritime Boundaries and EEZ (200NM) and augmentation of the Norwegian and Portuguese EEZ (black lines) which enclose within the yellow circles the LCHVF and LSHVF respectively. The red coloured areas represent the network of marine protected areas (MPAs). Edited maps from Flanders Marine Institute (2019) and OSPAR Network of MPAs (as of 1 October 2021)

The ISA is creating regulations for the resource exploration and development of "the Area" (Fig. 3). As imposed by the UN Convention of the Law of the Sea (UNCLOS), this governance system will incorporate a "financial mechanism" to distribute seafloor mineral exploitation benefits. This mechanism prioritises contractors' financial burdens over the environmental and socio-economic repercussions mentioned previously (Thiele & Singh, 2021). On the other hand, the Forum for Development and the Environment, which is an association of 50 different organisations (Seas_at_Risk, 2021), has released a statement calling for a “moratorium on mineral extraction on the seabed until thorough mapping of the ecosystems that will be affected, until we have overcome the environmental challenges associated with land-based mining, and until a proper assessment of the real societal need to open up the seabed for mineral extraction.”

However, as the saying goes: every law has its loophole. And in this case, it is the “Two-Year Rule” (Singh, 2022). This “rule” gives the ISA Council two years - until July 9, 2023 - to finalise legislation for mining minerals on the international seabed and equitably divide mining earnings and other benefits. The Council must "consider" and "provisionally approve" exploitation applications if the regulations are not adopted within this time. The “Two-Year Rule” was triggered by the small Pacific island nation of Nauru, on behalf of the mining company under their sponsorship, Nauru Ocean Resources Inc. (NORI) , which intends to submit for UNCLOS approval of a PoW for exploitation. The Metals Company (previously DeepGreen), a Canadian mining startup, owns 100% of Nauru-incorporated NORI.

7.2.4. Alternative approaches

A considerable number of the topics discussed in the preceding sections possess a high likelihood of materialising. Similar to other bureaucratic procedures, the expectation of timely implementation of regulations can often be perceived as overly optimistic or even compliant.

The pragmatic approach to this scenario would be to acknowledge that social and economic patterns are unlikely to undergo a significant shift in the immediate future. Thus, the extraction of mineral resources from the seabed will inevitably become necessary at some point in time. Therefore, certain research groups have proactively undertaken the task of specialising on offering alternatives to mitigate the impact of this inevitable endeavour.

Concurrently, there has been a surge in demand for new professionals in this particular field, leading to the emergence of educational programmes such as the one offered by NTNU (*Oceans pilot programme on deep-sea mining*). While the underlying motives of this programme stay unexamined, it is very likely that it will promote the development of creative and analytical professionals who possess the ability to make informed decisions based on a more comprehensive understanding, supported by empirical evidence, than their current counterpart. On the other hand, professionals in the field are currently developing innovative alternatives to the conventional approach of underwater mining. One such approach involves integrating traditional geological exploration techniques with geophysical approaches, such as seismic and electromagnetics, to detect dormant or extinct sulphide deposits and figure out how deep they are underneath the ocean floor (Koschinsky et al., 2018). Alternative proposals have been put forth, such as the implementation of robotic technology proposed by the North American Consortium for Responsible Ocean Mining (NACROM), as outlined on their official

website. This technology would enable the selective extraction of individual mineral resources, thereby reducing the environmental impact that has been previously discussed.

Given the aforementioned points, it is reasonable to state that adopting an interdisciplinary approach is strongly advisable. Thus, it becomes pertinent to consider the potential societal and economical implications that may arise from this activity in the future.

(Thiele & Singh, 2021) presents three clear points that encapsulate certain key socio-economic stances: At first, it is important that the financial system truly portrays all expenses and potential hazards linked to mining operations within the Area (Fig. 3). Secondly, indigenous, civil society and future generations must be considered as significant and representative as any other stakeholder. Secondly, it is imperative to acknowledge the importance and representation of indigenous communities, civil society, and future generations as stakeholders on par with any other interested group. Ultimately, this study aims to showcase the feasibility of implementing on a significant scale a payment regime designed with the interest of Humankind, particularly in developing nations. Such a regime has the potential to narrow the disparity between globalised economies and benefit those who have historically been marginalised.

In case the reader is interested in conducting additional research, some concepts that must be incorporated in the investigation include: Degrowth, Circular Economy, the “Let the minerals be” narrative, “the Two-Year rule”.

8. Conclusion

This thesis represents an initial step in using the potential of ML for the interpretation of deep-sea resources. The positive outcomes and functionality demonstrated by the three mosaics employed, while also highlighting the requisite degree of pre-processing necessary to ensure the reliable and adaptable application of machine learning algorithms. in this study highlight the value of ML in understanding and sustaining these unique ecosystems. While there are still limitations to be addressed and further research to be undertaken, the findings from this thesis helps to open the way for future advancements in the field.

Furthermore, it is important to note that the applicability of the results may be restricted to the particular geographical location under study, and it is advisable to use prudence when extending the outcomes to other deep-sea regions. Future work should attempt to expand on the number of landforms being mapped, and to separate between similar classes.

The utilization of mosaic and bathymetry datasets in this study exemplifies the importance of data diversity for ML-based mapping of deep-sea features. Incorporating additional types of datasets, can further enhance the accuracy and applicability of ML models in this domain. Furthermore, international cooperation and a multidisciplinary science approach are essential for comprehensively addressing the management of deep-sea resources.

As funding for long-term monitoring projects remains scarce, the cost of purchasing, implementing, and running AI technology continues to decrease, making automation an attractive alternative for conservation management in marine ecosystems.

From an ethical standpoint, deep sea mining raises concerns due to knowledge gaps, environmental repercussions and its current state of development. Limited understanding of deep-sea ecosystems necessitates precautionary measures to avoid irreversible damage. Environmental consequences, including habitat destruction and species extinction, raise ethical concerns for present and future generations. Addressing knowledge gaps through baseline studies and ongoing monitoring is crucial. Transparent and accountable governance, with international cooperation, can mitigate risks. Alternative approaches such as circular economy principles, recycling, and sustainable practices can reduce the demand for deep-sea mining. International collaboration and the share of knowledge can result in comprehensive and sustainable solutions. Ethical decision-making must balance economic interests with the preservation of deep-sea biodiversity, ensuring long-term well-being for marine ecosystems and the human society that relies from them.

References list / Source of data

Alt, J. C. (1995). Subseafloor processes in mid-ocean ridge hydrothennal systems. *Washington DC American Geophysical Union Geophysical Monograph Series*, *91*, 85-114. https://doi.org/10.1029/GM091p0085

Ardito, G., & Rovere, M. (2022). Racing the clock: Recent developments and open environmental regulatory issues at the International Seabed Authority on the eve of deep-sea mining. *Marine Policy*, *140*, 105074. https://doi.org/https://doi.org/10.1016/j.marpol.2022.105074

Barreyre, T., Escartín, J., García, R., Cannat, M., Mittelstaedt, E. L., & Prados, R. (2012). Structure, temporal evolution, and heat flux estimates from the Lucky Strike deep-sea hydrothermal field derived from seafloor image mosaics. *Geochemistry*, *13*. https://sci-hub.se/10.1029/2011gc003990

Blanchard, C., Harrould-Kolieb, E., Jones, E., & Taylor, M. (2023). The current status of deep-sea mining governance at the International Seabed Authority. *Marine Policy*, *147*, 105396. https://doi.org/10.1016/j.marpol.2022.105396

Blaschke, T., Hay, G. J., Kelly, M., Lang, S., Hofmann, P., Addink, E., Queiroz Feitosa, R., van der Meer, F., van der Werff, H., van Coillie, F., & Tiede, D. (2014). Geographic Object-Based Image Analysis – Towards a new paradigm. *ISPRS Journal of Photogrammetry and Remote Sensing*, *87*, 180-191. https://doi.org/https://doi.org/10.1016/j.isprsjprs.2013.09.014

Bramley, J. M., Berit, L., Adeline, M. D., Sofia, M., Alba, G., Iain, J. S., Fernando, J. A. S. B., Jörg, B., Anke, D., Mark, E. V., Laurence, J. N., Isobel, A. L. M. Y., Paul, A. J. L., & Sven, P. (2019). Geological fate of seafloor massive sulphides at the TAG hydrothermal field (Mid-Atlantic Ridge). *Ore Geology Reviews*, *107*, 903-925. https://doi.org/https://doi.org/10.1016/j.oregeorev.2019.03.005

Brundage, W., & Patterson, R. (1976). LIBEC photography as a sea floor mapping tool. OCEANS'76,

Burke, K. (1976). Development of Graben Associated with the Initial Ruptures of the Atlantic Ocean. In M. H. P. Bott (Ed.), *Developments in Geotectonics* (Vol. 12, pp. 93-112). Elsevier. https://doi.org/https://doi.org/10.1016/B978-0-444-41549-3.50011-6

Burke, K. C., & Wilson, J. T. (1976). Hot Spots on the Earth's Surface. *Scientific American*, *235*(2), 46-59. http://www.jstor.org/stable/24950416

Christiansen, B., Denda, A., & Christiansen, S. (2020). Potential effects of deep seabed mining on pelagic and benthopelagic biota. *Marine Policy*, *114*, 103442. https://doi.org/https://doi.org/10.1016/j.marpol.2019.02.014

Church, C., & Crawford, A. (2020). Minerals and the Metals for the Energy Transition: Exploring the Conflict Implications for Mineral-Rich, Fragile States. In M. Hafner & S. Tagliapietra (Eds.), *The Geopolitics of the Global Energy Transition* (pp. 279-304). Springer International Publishing. https://doi.org/10.1007/978-3-030-39066-2_12

Clark, M. R., Durden, J. M., & Christiansen, S. (2020). Environmental Impact Assessments for deep-sea mining: Can we improve their future effectiveness? *Marine Policy*, *114*. https://doi.org/https://doi.org/10.1016/j.marpol.2018.11.026

Cohen, C. J. (2000). *Early History of Remote Sensing* 2013 IEEE Applied Imagery Pattern Recognition Workshop (AIPR), https://doi.ieeecomputersociety.org/10.1109/AIPRW.2000.953595

Cuyvers, L., Berry, W., Gjerde, K., Thiele, T., & Wilhem, C. (2018). *Deep Seabed Mining, a Rising Environmental Challenge*. IUCN Gland, Switzerland.

Dick, H., Lin, J., & Schouten, H. (2003). An ultraslow-spreading class of ocean ridge. *Nature*, *426*, 405-412. https://doi.org/10.1038/nature02128

Directorate, P. (2023). Resource assessment seabed minerals.

Ditria, E. M., Buelow, C. A., Gonzalez-Rivero, M., & Connolly, R. M. (2022). Artificial intelligence and automated monitoring for assisting conservation of marine ecosystems: A perspective [Review]. *Frontiers in Marine Science*, *9*. https://doi.org/10.3389/fmars.2022.918104

Dover, C. L. v. (1995). Ecology of mid-Atlantic ridge hydrothermal vents. *Geological Society, London, Special Publications*, *87*(1), 257-294. https://sci-hub.se/10.1144/gsl.sp.1995.087.01.21

Drazen, J. C., Smith, C. R., Gjerde, K. M., Haddock, S. H. D., Carter, G. S., Choy, C. A., Clark, M. R., Dutrieux, P., Goetze, E., Hauton, C., Hatta, M., Koslow, J. A., Leitner, A. B., Pacini, A., Perelman, J. N., Peacock, T., Sutton, T. T., Watling, L., & Yamamoto, H. (2020). Midwater ecosystems must be considered when evaluating environmental risks of deep-sea mining. *Proceedings of the National Academy of Sciences*, *117*(30), 17455-17460. https://doi.org/doi:10.1073/pnas.2011914117

Dyment, J., Lin, J., & Baker, E. T. (2007). RIDGE-HOTSPOT INTERACTIONS

What Mid-Ocean Ridges Tell Us About Deep Earth Processes. *Oceanography*, *20*(1), 102-115. http://www.jstor.org/stable/24859979

Eason, D., Dunn, R., Canales, J., & Sohn, R. (2016). Segment-scale variations in seafloor volcanic and tectonic processes from multibeam sonar imaging, Mid-Atlantic Ridge Rainbow region (35°45'-36°35'N). *Geochemistry, Geophysics, Geosystems*, *17*. https://doi.org/10.1002/2016GC006433

Emery, K. O., & Uchupi, E. (2012). *The geology of the Atlantic Ocean*. Springer Science & Business Media.

Escartin, J., Cannat, M., & Deschamps, A. (2021). *Microbathymetry from AUV and ROV Surveys (MOMARETO'06, MOMAR'08-Leg1 and BATHYLUCK'09 cruises) along the Lucky Strike ridge segment (Mid Atlantic Ridge)* SEANOE. https://doi.org/10.17882/80574

Escartín, J., Garcia, R., Delaunoy, O., Ferrer, J., Gracias, N., Elibol, A., Cufi, X., Neumann, L., Fornari, D., & Humphris, S. (2008). Globally aligned photomosaic of the Lucky Strike hydrothermal vent field (Mid-Atlantic Ridge, 37 18.5' N): Release of georeferenced data, mosaic construction, and viewing software. *Geochemistry, Geophysics, Geosystems*, *9*(12). https://sci-hub.se/10.1029/2008GC002204

Escartin J., B. T., Cannat M., Garcia R., Gracias N., Deschamps A., Salocchi A., Sarradin Pierre-Marie, Ballu V. (2015). Hydrothermal activity along the slow-spreading Lucky Strike ridge segment (Mid-Atlantic Ridge): Distribution, heatflux, and geological controls. *Earth and Planetary Science Letters*, *431*, 173-185. https://doi.org/10.1016/j.epsl.2015.09.025

Fisher, C. R., Takai, K. E. N., & Le Bris, N. (2007). Hydrothermal Vent Ecosystems. *Oceanography*, *20*(1), 14-23. http://www.jstor.org/stable/24859970

Fox, P. J., Schreiber, E., & Peterson, J. (1973). The geology of the oceanic crust: compressional wave velocities of oceanic rocks. *Journal of Geophysical Research*, *78*(23), 5155-5172.

Gentemann, C. L., Scott, J. P., Mazzini, P. L. F., Pianca, C., Akella, S., Minnett, P. J., Cornillon, P., Fox-Kemper, B., Cetinić, I., Chin, T. M., Gomez-Valdes, J., Vazquez-Cuervo, J., Tsontos, V., Yu, L., Jenkins, R., De Halleux, S., Peacock, D., & Cohen, N. (2020). Saildrone: Adaptively Sampling the Marine Environment. *Bulletin of the American Meteorological Society*, *101*(6), E744-E762. https://doi.org/https://doi.org/10.1175/BAMS-D-19-0015.1

Geospatial, T. (2023). eCognition Software product description. https://docs.ecognition.com/v9.5.0/Page collection/eCognition Suite Documentation.htm?tocpath =Documentation eCognition Suite%7C_____0

German, C., M, T., Knoery, J., Jean-luc, C., Jean-Baptiste, P., & N, E. (2010). Heat, volume and chemical fluxes from submarine venting: A synthesis of results from the Rainbow hydrothermal field, 36 degrees N MAR. *Deep-sea Research Part I-oceanographic Research Papers (0967-0637) (Pergamon-elsevier Science Ltd), 2010-04 , Vol. 57 , N. 4 , P. 518-527*, *57*. https://doi.org/10.1016/j.dsr.2009.12.011

Gini, C., Escartín, J., Cannat, M., & Barreyre, T. (2021). Extrusive upper crust formation at slow-spreading ridges: Fault steering of lava flows. *Earth and Planetary Science Letters*, *576*, 117202. https://doi.org/https://doi.org/10.1016/j.epsl.2021.117202

Guo, X., Fan, N., Liu, Y., Liu, X., Wang, Z., Xie, X., & Jia, Y. (2023). Deep seabed mining: Frontiers in engineering geology and environment. *International Journal of Coal Science & Technology*, *10*(1), 23. https://doi.org/10.1007/s40789-023-00580-x

Gupta, N., & Bhadauria, H. S. (2014). Object based Information Extraction from High Resolution Satellite Imagery using eCognition. *International Journal of Computer Science Issues (IJCSI)*, *11*(3), 139-144. https://www.proquest.com/scholarly-journals/object-based-information-extraction-high/docview/1540085882/se-2?accountid=8579

http://openurl.bibsys.no/openurl?url_ver=Z39.88-2004&rft_val_fmt=info:ofi/fmt:kev:mtx:journal&genre=article&sid=ProQ:ProQ%3Amaterialsscijournals&atitle=Object+based+Information+Extraction+from+High+Resolution+Satellite+Imagery+using+eCognition&title=International+Journal+of+Computer+Science+Issues+%28IJCSI%29&issn=16940814&date=2014-05-01&volume=11&issue=3&spage=139&au=Gupta%2C+Neha%3BBhadauria%2C+H+S&isbn=&jtitle=International+Journal+of+Computer+Science+Issues+%28IJCSI%29&btitle=&rft_id=info:eric/&rft_id=info:doi/

Hallgren, A., & Hansson, A. (2021). Conflicting narratives of deep sea mining. *Sustainability*, *13*(9), 5261.

Hossain, M. D., & Chen, D. (2019). Segmentation for Object-Based Image Analysis (OBIA): A review of algorithms and challenges from remote sensing perspective. *ISPRS Journal of Photogrammetry and Remote Sensing*, *150*, 115-134. https://doi.org/https://doi.org/10.1016/j.isprsjprs.2019.02.009

Humphris, S. E., Fornari, D. J., Scheirer, D. S., German, C. R., & Parson, L. M. (2002). Geotectonic setting of hydrothermal activity on the summit of Lucky Strike Seamount (37°17′N, Mid-Atlantic Ridge). *Geochemistry, Geophysics, Geosystems*, *3*(8), 1-25. https://doi.org/https://doi.org/10.1029/2001GC000284

Jaeschke, A., Jørgensen, S., Bernasconi, S., Pedersen, R., Thorseth, I., & Früh-Green, G. (2012). Microbial diversity of Loki's Castle black smokers at the Arctic Mid-Ocean Ridge. *Geobiology*, *10*, 548-561. https://doi.org/10.1111/gbi.12009

Jiang, M., & Zhu, Z. (2022). The Role of Artificial Intelligence Algorithms in Marine Scientific Research [Opinion]. *Frontiers in Marine Science*, *9*. https://doi.org/10.3389/fmars.2022.920994

Kelley, D., Karson, J., Fornari, D., Perfit, M., & Shank, T. (2015). *Discovering the Deep: A Photographic Atlas of the Seafloor and Ocean Crust*. https://doi.org/10.1017/CBO9781139050524

Kelley, D. S., & Shank, T. M. (2010). Hydrothermal systems: A decade of discovery in slow spreading environments. *Diversity of hydrothermal systems on slow Spreading ocean ridges*, *188*, 369-407. https://sci-hub.se/10.1029/2010GM000945

Keohane, I., & White, S. (2022). Chimney Identification Tool for Automated Detection of Hydrothermal Chimneys from High-Resolution Bathymetry Using Machine Learning. *Geosciences*, *12*(4), 176.

Koschinsky, A., Heinrich, L., Boehnke, K., Cohrs, J. C., Markus, T., Shani, M., Singh, P., Smith Stegen, K., & Werner, W. (2018). Deep-sea mining: Interdisciplinary research on potential environmental, legal, economic, and societal implications. *Integr Environ Assess Manag*, *14*(6), 672-691. https://doi.org/10.1002/ieam.4071

Langmuir, C., Humphris, S., Fornari, D., Van Dover, C., Von Damm, K., Tivey, M., Colodner, D., Charlou, J.-L., Desonie, D., & Wilson, C. (1997). Hydrothermal vents near a mantle hot spot: the Lucky Strike vent field at 37 N on the Mid-Atlantic Ridge. *Earth and Planetary Science Letters*, *148*(1-2), 69-91. https://sci-hub.se/10.1016/s0012-821x(97)00027-7

LeCun, Y., Bengio, Y., & Hinton, G. (2015). Deep learning. *Nature*, *521*(7553), 436-444. https://doi.org/10.1038/nature14539

Levin, L. A., Bett, B. J., Gates, A. R., Heimbach, P., Howe, B. M., Janssen, F., McCurdy, A., Ruhl, H. A., Snelgrove, P., Stocks, K. I., Bailey, D., Baumann-Pickering, S., Beaverson, C., Benfield, M. C., Booth, D. J., Carreiro-Silva, M., Colaço, A., Eblé, M. C., Fowler, A. M., . . . Weller, R. A. (2019). Global Observing Needs in the Deep Ocean [Review]. *Frontiers in Marine Science*, *6*. https://doi.org/10.3389/fmars.2019.00241

Mayer, L. A. (2006). Frontiers in Seafloor Mapping and Visualization. *Marine Geophysical Researches*, *27*(1), 7-17. https://doi.org/10.1007/s11001-005-0267-x

McVeigh, K. (2023). Row erupts over deep-sea mining as world races to finalise vital regulations. *The Guardian*.

Menini, E., & Van Dover, C. L. (2019). An atlas of protected hydrothermal vents. *Marine Policy*, *108*, 103654. https://doi.org/https://doi.org/10.1016/j.marpol.2019.103654

Miller, K. A., Thompson, K. F., Johnston, P., & Santillo, D. (2018). An Overview of Seabed Mining Including the Current State of Development, Environmental Impacts, and Knowledge Gaps [Review]. *Frontiers in Marine Science*, *4*. https://doi.org/10.3389/fmars.2017.00418

Mitchell, N. (2018). *Mid-ocean Ridges*. https://doi.org/10.1007/978-3-319-57852-1_18

Nicholls, G. D., Nalwalk, A. J., & Hays, E. E. (1964). The nature and composition of rock samples dredged from the Mid-Atlantic Ridge between 22°N and 52°N. *Marine Geology*, *1*(4), 333-343. https://doi.org/https://doi.org/10.1016/0025-3227(64)90019-2

Nussbaum, S., Menz, G., Nussbaum, S., & Menz, G. (2008). eCognition image analysis software. *Object-Based Image Analysis and Treaty Verification: New Approaches in Remote Sensing–Applied to Nuclear Facilities in Iran*, 29-39.

Ondréas, H., Cannat, M., Fouquet, Y., Normand, A., Sarradin, P. M., & Sarrazin, J. (2009). Recent volcanic events and the distribution of hydrothermal venting at the Lucky Strike hydrothermal field, Mid-Atlantic Ridge. *Geochemistry, Geophysics, Geosystems*, *10*(2). https://doi.org/https://doi.org/10.1029/2008GC002171

Palgan, D. (2017). *Volcano-tectonic controls of hydrothermalism on a hot spot-influenced mid-ocean ridge: Insights from Iceland and Reykjanes Ridge* Christian-Albrechts-Universität].

Pedersen, R. B., Rapp, H. T., Thorseth, I. H., Lilley, M. D., Barriga, F. J. A. S., Baumberger, T., Flesland, K., Fonseca, R., Früh-Green, G. L., & Jorgensen, S. L. (2010). Discovery of a black smoker vent field and vent fauna at the Arctic Mid-Ocean Ridge. *Nature Communications*, *1*(1), 126. https://doi.org/10.1038/ncomms1124

Puzenat, V., Escartin, J., Martelat, J.-E., Barreyre, T., Bauer, S. L. M., Nomikou, P., Gracias, N., Allemand, P., Antoniou, V., & Coskun, O. (2021). Shallow-water hydrothermalism at Milos (Greece): Nature, distribution, heat fluxes and impact on ecosystems. *Marine Geology*, *438*, 106521.

Ricard Prados, R. G., Nuno Gracias, Javier Escartín, and László Neumann. (2012). A Novel Blending Technique for Underwater Gigamosaicing. *OCEANIC ENGINEERING*, *VOL. 37, NO. 4*, pp. 626-644. https://doi.org/10.1109/JOE.2012.2204152

Robson, B., Nuth, C., Dahl, S., Hölbling, D., Strozzi, T., & Nielsen, P. (2015). Automated classification of debris-covered glaciers combining optical, SAR and topographic data in an object-based environment. *Remote Sensing of Environment*, *170*, 372-387. https://doi.org/10.1016/j.rse.2015.10.001

Robson, B. A., Bolch, T., MacDonell, S., Hölbling, D., Rastner, P., & Schaffer, N. (2020). Automated detection of rock glaciers using deep learning and object-based image analysis. *Remote Sensing of Environment*, *250*, 112033. https://doi.org/https://doi.org/10.1016/j.rse.2020.112033

Robson, B. A., Hölbling, D., Nuth, C., Strozzi, T., & Dahl, S. O. (2016). Decadal Scale Changes in Glacier Area in the Hohe Tauern National Park (Austria) Determined by Object-Based Image Analysis. *Remote Sensing*, *8*(1), 67. https://www.mdpi.com/2072-4292/8/1/67

Seas_at_Risk. (2021). At a crossroads: Europe's role in deep-sea mining.

Seton, M., Müller, D., Zahirovic, S., Williams, S., Wright, N., Cannon, J., Whittaker, J., Matthews, K., & McGirr, R. (2020). A Global Data Set of Present-Day Oceanic Crustal Age and Seafloor Spreading Parameters. *Geochemistry, Geophysics, Geosystems*, *21*. https://doi.org/10.1029/2020GC009214

Singh, P. A. (2022). The Invocation of the 'Two-Year Rule' at the International Seabed Authority: Legal Consequences and Implications. *The International Journal of Marine and Coastal Law*, *37*(3), 375-412. https://doi.org/https://doi.org/10.1163/15718085-bja10098

Snook, B., Drivenes, K., Rollinson, G. K., & Aasly, K. (2018). Characterisation of Mineralised Material from the Loki's Castle Hydrothermal Vent on the Mohn's Ridge. *Minerals*, *8*(12), 576. https://www.mdpi.com/2075-163X/8/12/576

Somoza, L., Medialdea, T., González, F. J., Machancoses, S., Candón, J. A., Cid, C., Calado, A., Afonso, A., Pinto Ribeiro, L., Blasco, I., Albuquerque, M., Asensio-Ramos, M., Bettencourt, R., De Ignacio, C., López-Pamo, E., Ramos, B., Rincón-Tomás, B., Santofimia, E., Souto, M., . . . Madureira, P. (2021). High-resolution multibeam bathymetry of the northern Mid-Atlantic Ridge at 45–46° N: the Moytirra hydrothermal field. *Journal of Maps*, *17*(2), 184-196. https://doi.org/10.1080/17445647.2021.1898485

Sonogashira, M., Shonai, M., & Iiyama, M. (2020). High-resolution bathymetry by deep-learning-based image superresolution. *PLOS ONE*, *15*(7), e0235487. https://doi.org/10.1371/journal.pone.0235487

Thiele, T., & Singh, P. (2021). A Comprehensive Approach to the Payment Mechanism for Deep Seabed Mining. https://doi.org/10.48440/iass.2021.004

Timilsina, S., Sharma, S., & Aryal, J. (2019). MAPPING URBAN TREES WITHIN CADASTRAL PARCELS USING AN OBJECT-BASED CONVOLUTIONAL NEURAL NETWORK. *ISPRS Annals of Photogrammetry, Remote Sensing and Spatial Information Sciences*, *IV-5/W2*, 111-117. https://doi.org/10.5194/isprs-annals-IV-5-W2-111-2019

Tivey, M. K. (2007). Generation of Seafloor Hydrothermal Vent Fluids and Associated Mineral Deposits. *Oceanography*, *20*(1), 50-65. http://www.jstor.org/stable/24859975

Van Dover, C. L., Colaço, A., Collins, P. C., Croot, P., Metaxas, A., Murton, B. J., Swaddling, A., Boschen-Rose, R. E., Carlsson, J., Cuyvers, L., Fukushima, T., Gartman, A., Kennedy, R., Kriete, C., Mestre, N. C., Molodtsova, T., Myhrvold, A., Pelleter, E., Popoola, S. O., . . . Vermilye, J. (2020). Research is needed to inform environmental management of hydrothermally inactive and extinct polymetallic sulfide (PMS) deposits. *Marine Policy*, *121*, 104183. https://doi.org/https://doi.org/10.1016/j.marpol.2020.104183

Wölfl, A.-C., Snaith, H., Amirebrahimi, S., Devey, C. W., Dorschel, B., Ferrini, V., Huvenne, V. A. I., Jakobsson, M., Jencks, J., Johnston, G., Lamarche, G., Mayer, L., Millar, D., Pedersen, T. H., Picard, K., Reitz, A., Schmitt, T., Visbeck, M., Weatherall, P., & Wigley, R. (2019). Seafloor Mapping – The Challenge of a Truly Global Ocean Bathymetry [Review]. *Frontiers in Marine Science*, *6*. https://doi.org/10.3389/fmars.2019.00283

Ye, J. H. X. (2022). Real-time Underwater 3D Reconstruction Method Based on Stereo Camera. *International Conference on Mechatronics and Automation (ICMA)*, 1204-1209. https://doi.org/10.1109/ICMA54519.2022.9855905

Zeng, Z., Chen, Z., Zhang, Y., & Li, X. (2020). Geological, physical, and chemical characteristics of seafloor hydrothermal vent fields. *Journal of Oceanology and Limnology*, *38*, 985-1007. https://doi.org/10.1007/s00343-020-0123-5